JOURNAL OF RHEOLOGY®

Dynamic shear rheology of a thixotropic suspension: Comparison of an improved structure-based model with large amplitude oscillatory shear experiments

Matthew J. Armstrong, Antony N. Beris, Simon A. Rogers, and Norman J. Wagner

Citation: Journal of Rheology **60**, 433 (2016); doi: 10.1122/1.4943986
View online: http://dx.doi.org/10.1122/1.4943986
View Table of Contents: http://scitation.aip.org/content/sor/journal/jor2/60/3?ver=pdfcov
Published by the The Society of Rheology

Articles you may be interested in

Large amplitude oscillatory shear of the Giesekus model
J. Rheol. **60**, 257 (2016); 10.1122/1.4941423

Yielding processes in a colloidal glass of soft star-like micelles under large amplitude oscillatory shear (LAOS)
J. Rheol. **54**, 1219 (2010); 10.1122/1.3483610

Structural analysis of non-aqueous layered silicate suspensions subjected to shear flow
J. Rheol. **53**, 1025 (2009); 10.1122/1.3193720

Oscillatory shear of suspensions of noncolloidal particles
J. Rheol. **50**, 711 (2006); 10.1122/1.2234366

Response of concentrated suspensions under large amplitude oscillatory shear flow
J. Rheol. **49**, 71 (2005); 10.1122/1.1814112

Redistribution subject to SOR license or copyright; see http://scitation.aip.org/content/sor/journal/jor2/info/about. Downloaded to IP: 128.175.82.78 On: Fri, 01 Apr 2016 15:11:45

Dynamic shear rheology of a thixotropic suspension: Comparison of an improved structure-based model with large amplitude oscillatory shear experiments

Matthew J. Armstrong,[a] Antony N. Beris, Simon A. Rogers,[b] and Norman J. Wagner[c]

Department of Chemical and Biomolecular Engineering, University of Delaware, Newark, Delaware 19716

(Received 6 August 2015; final revision received 29 February 2016; published 29 March 2016)

Abstract

Rheological measurements on a model thixotropic suspension by Dullaert and Mewis [J. Non-Newtonian Fluid Mech. **139**(1–2), 21–30 (2006); Rheol. Acta **45**, 23–32 (2005)] are extended to include large amplitude oscillatory shear (LAOS) flow, shear flow reversal, and a novel unidirectional LAOS flow to provide an extended rheological data set for testing constitutive models. We use this extended data set to test a new structure-based model developed by improving the Delaware thixotropic model [A. Mujumdar *et al*., J. Non-Newtonian Fluid Mech. **102**, 157–178 (2002); A. J. Apostolidis *et al*., J. Rheol. **59**, 275–298 (2015)]. Model parameters are determined from steady, small amplitude oscillatory, and step shear rate tests. Holding those parameters fixed, model predictions are compared to LAOS experiments. Similar comparisons are made for three contemporary models from the literature. Two of these models use a scalar internal structural parameter and include the modified Jeffreys model proposed by de Souza Mendes and Thompson [Rheol. Acta **52**, 673–694 (2013)]. The third model is based on fluidity additivity [F. Bautista *et al*., J. Non-Newtonian Fluid Mech. **80**, 93–113 (1999)]. A common weakness in all models is shown to be the use of scalar order parameters that cannot account for the reversal of flow directionality inherent in LAOS flow. This is further illustrated by comparison with flow reversal and unidirectional LAOS experiments. © *2016 The Society of Rheology*.
[http://dx.doi.org/10.1122/1.4943986]

I. INTRODUCTION

"Thixotropy is defined as the continuous decrease of viscosity with time when flow is applied to a sample that has been previously at rest, and the subsequent recovery of viscosity when the flow is discontinued" [1]. "Ideal thixotropy" refers to a "time-dependent viscous response to the history of the strain rate with fading memory of that history" [2]. It is generally accepted that thixotropic suspensions have an underlying microstructure that reversibly breaks down under shear flow and rebuilds upon its cessation [3–17]. Typical thixotropic suspensions comprise colloidal particles, aggregates, or flocs that associate at rest, and are broken apart upon an applied shear flow. For an ideal thixotropic suspension, the stress relaxes immediately upon flow cessation because such suspensions are dominated by viscous hydrodynamic interactions. However, real suspensions sometimes exhibit additional features characteristic of nonlinear viscoelasticity, such that one can differentiate between "ideal" and "nonideal" thixotropic materials, the latter having an additional viscoelastic time scale for stress relaxation.

Thixotropic suspensions are ubiquitous to everyday life and in industry. Many food products, paints, cleaning, and industrial waste products are thixotropic [4,11,13,14]. Blood is also a thixotropic suspension [15–17], and several thixotropic models have been proposed to model its flow, most recently by Apostolidis *et al*. [6]. Finally, there are several multibillion dollar superfund site cleanup efforts underway at two national labs based on the remediation of highly thixotropic suspensions containing transuranic waste [13].

Generally speaking, thixotropic models can be categorized into three broad classes with increasing order of microstructure resolution (and hence, complexity): A phenomenological continuum approach, a phenomenological structural kinetics model approach, and a particle-level microstructural approach. The structural kinetics approach balances the simplicity of the continuum approach with a simplified, phenomenological model for structure against the complexity of a more fundamental model based on particle micromechanics. As such, structure-kinetics models attempt to capture the key features of the coupling of material properties to structure while avoiding computational intractability when applied to time-dependent and complex flows. Necessarily this involves introducing parameters for various structure building and breaking phenomena, as well as functional forms relating viscous and elastic material properties to the structure parameter. Such phenomenological parameters can, in principle, be derived by coarse graining the more fundamental, particle micromechanics equations [18,19].

The modeling of thixotropy can trace its roots to Goodeve's treatise on the relationship between thixotropy and structure [20]. In this work, a simple structural kinetics model is postulated that links the change in a scalar structure parameter to shear forces acting on a microstructure. Since then many others have built on this framework and much of this is surveyed in reviews [1,11,21]. In most of these approaches, the structure is described by a scalar parameter

[a]Present address: Department of Chemistry and Life Science, United States Military Academy, West Point, New York 10996.
[b]Present address: Department of Chemical and Biomolecular Engineering, University of Illinois Urbana-Champaign, Champaign, Illinois 61801.
[c]Author to whom correspondence should be addressed; electronic mail: wagnernj@udel.edu

© 2016 by The Society of Rheology, Inc.

Redistribution subject to SOR license or copyright; see http://scitation.aip.org/content/sor/journal/jor2/info/about. Downloaded to IP: 128.175.82.78 On: Fri, 01 Apr 2016 15:11:45

with values typically ranging between 0 and 1 [9,10,22,23]. A structural value of one corresponds to the fully structured material and a value of zero is indicative of the complete absence of structure due to deformational breakdown processes. The range of approaches to structural kinetic modeling is very broad and alternative formulations abound [7,24–26].

Scalar structure-based models of the response of thixotropic materials to flow incorporate a parameter, usually denoted as λ, to represent the "degree of structure" with an associated equation describing its evolution with time and shear conditions. Early work by Goodeve associated the structure parameter with degree of "bonding" between particles or aggregates in the suspension [20], but in general, this parameter does not have a quantifiable microstructural interpretation. In some cases, such as the modified Jeffreys model, [7,27] the structural parameter is allowed to range over a broader range and can take on any positive value. Other formulations are possible, such as the Bautista–Monero–Puig model (BMPM) [6], which uses the fluidity as a surrogate for the structure based on work of Fredrickson [23]. Experimentally, structure can be measured directly under flow through the use of structure-sensitive techniques such as X-ray scattering or small angle neutron scattering under flow, [9,28,29], small angle light scattering under flow [30,31] and confocal microscopy under flow [32,33], although no firm connections to the scalar structure order parameter have been identified to date.

The structure parameter satisfies a kinetic, evolution equation that combines physical processes acting to build or break the suspension microstructure. In the limit of infinitely high shear rates, the microstructure in a thixotropic suspension goes to zero, which represents a state of complete microstructure breakdown. Upon flow cessation the microstructure rebuilds through processes such as Brownian motion, which may be diffusion or reaction limit [34]. During flow, shear-induced aggregation and Brownian aggregation compete with shear-breakage [34,35]. Various models have been proposed for each of these processes in terms of the structure parameter, and combining them leads to an ordinary differential equation for the time evolution of the structure parameter under shear flow [1,9,36].

Structural evolution equations have been developed that focus on the difference between the present state of structure and an equilibrium state [5,7,9,10]. Recently, Dimitriou *et al*. [37] made several insightful contributions to modeling thixotropic, elastoviscoplastic (EVP) materials by decomposing the strain and shear rate into elastic and plastic components, building on work by de Souza Mendes and Thompson [7,24]. This technique assigns the appropriate component of strain and shear rate to specific rheological behavior, i.e., elastic (reversible, recoverable) behavior, and plastic (irreversible, dissipative) behavior. With regards to structure, the elastic component is associated with structure "stretching" and recovery, and the plastic component is associated with structure destruction and rebuilding [3,6,24,37]. We incorporate aspects of these works by developing a new structure-based model we refer to as the modified Delaware thixotropic model (MDTM).

Recently, similar structural evolution equations have been coupled to more complicated, tensorial constitutive equations. In particular Giacomin and Dealy [38], and Jacob *et al*. [39], involved modified versions of the Maxwell and Giesekus models, respectively. In these tensorial approaches, the structure parameter λ remains a scalar parameter with a range of values between zero and one. Other recent work modeling of elasto-visco-plastic, or EVP materials, by Stickel *et al*. [40] uses a modified version of the EVP model of Cheddadi *et al*. [41] and Saramito [42]. We find that the EVP model cannot capture the thixotropic time scales inherent in our material due to the fact that it only has a viscoelastic time scale. The Blackwell and Ewoldt model [43], based on a Jeffreys framework, does not have a yield stress term, and therefore cannot fit our steady state data. However, we believe that it could, by adding a yield stress term, or using it in "multimode" form, and fitting the mode parameters directly to the small amplitude oscillatory shear (SAOS) frequency sweep data first, similar to the way we used the BMPM here (results shown in Sec. IV B and in Supplementary Material [44]) [43].

Generally, structure-kinetics models have been fit and validated against steady viscosity measurements combined with some time-dependent flows, such as steps up and down in shear rate. More recently, structural kinetics models have been applied to other time-dependent shear flows such as large amplitude oscillatory shear (LAOS) flow [3,5,7,10]. In a LAOS test, a sinusoidal strain with specified amplitude and frequency is applied, which can be independently varied to explore material response over a broad range of deformation amplitudes and timescales. Early examples of LAOS include work by Philoppoff to rheologically characterize viscoelastic materials [38,45]. Modern studies of LAOS combine rheological measurements with simultaneous measurements of microstructure [46,47–49]. In the absence of such direct evidence for the microstructural behavior under LAOS a number of techniques have been proposed to interpret the material's microstructure response during LAOS from the rheology alone [38,47,50–52]. Such interpretations benefit from having robust and accurate structure-based constitutive models that are applicable to results from LAOS, which could further enable fitting LAOS measurements to predict material performance under other flow conditions [43,53,54]. Further developing and validating this capability for thixotropic suspensions is an important part of the work presented here.

In the following we investigate the ability of structure-parameter based, thixotropic models to predict LAOS experiments conducted on a model thixotropic material. In Sec. II, we introduce the structure-based model for thixotropic suspensions, termed the MDTM, and compare it against other models from literature. The model, thixotropic suspension used and the rheological tests conducted are presented, along with the model parameter fitting in Sec. III. In Sec. IV, we present the LAOS experiments along with a comparison model predictions. We compare and contrast the models Sec. V and present our conclusions in Sec. VI.

Redistribution subject to SOR license or copyright; see http://scitation.aip.org/content/sor/journal/jor2/info/about. Downloaded to IP: 128.175.82.78 On: Fri, 01 Apr 2016 15:11:45

II. THIXOTROPY MODELS

Three thixotropic models used in this work are, in order of increasing complexity: the simple scalar thixotropy model (SSTM) presented in Chap. 7 of, "Colloidal Suspension Rheology," [9]; a modification of the Delaware thixotropy model, as originally derived by Mujumdar *et al.* [5] presented in detail in the following; and a modified Jeffreys model, known as the "unified-approach" model (UAM) from de Souza Mendes and Thompson [7]. Each of these models has a scalar parameter that represents the structure, λ, an evolution equation for structure in the form of an ordinary differential equation, as well as a constitutive equation for the stress in terms of elastic and viscous contributions. The fourth model examined in this investigation is from BMPM [8], and is a tensorial model based the evolution of inverse viscosity (fluidity) modes entering the description of a modified multimodal Maxwell model. Fitting and predictions obtained for these three models are discussed in Sec. V, and to be found in more detail in the accompanying Supplementary Material [44].

In the simple scalar thixotropic (SST) and MDTM, the total shear stress in shear flows is decomposed into an elastic stress, σ_e and viscous stress σ_v, both of which are functions of the current level of microstructure λ

$$\sigma_{\text{tot}} = \sigma_e(\lambda) + \sigma_v(\lambda). \tag{1}$$

This respects the fundamentally different micromechanical sources of the stresses arising from hydrodynamic and interparticle interactions, respectively [55]. Alternatively, the UAM and BMP models use a modified Jeffreys and Maxwell constitutive equation, respectively, for the deviatoric stress $\boldsymbol{\sigma}$ [7,27,56]

$$\boldsymbol{\sigma} + \frac{\eta(\lambda)}{G(\lambda)}\dot{\boldsymbol{\sigma}} = \eta(\lambda)\dot{\boldsymbol{\gamma}} \tag{2}$$

is the governing equation of the Maxwell model, where the elastic modulus G, and the current viscosity, η, are both modified to be functions of λ. A detailed description of the model is offered here for the MDTM, as this is new. For completion, descriptions for all others are included in the Supplementary Material [44]. The Jeffreys model is similar to the Maxwell model, Eq. (2), with an additional characteristic time of material loading included [27].

A. Modified Delaware thixotropy model

The MDTM evolved from the original "Delaware model" [3], which was in turn a modification of the original Herschel–Bulkley model [9]. The original Delaware thixotropic model consisted of the Herschel–Bulkley stress expression with material properties dependent upon a scalar parameter to describe the current level of structure. In the MDTM an additional term was added to the structure evolution equation to account for shear aggregation processes, following the approach of Dullaert and Mewis [3]. The new term introduces an additional time scale and an additional power law exponent

$$\frac{d\lambda}{dt} = k_{\text{Brown}}\left[-\lambda|\hat{t}_{r1}\dot{\gamma}_p|^a + (1-\lambda)\left(1+|\hat{t}_{r2}\dot{\gamma}_p|^d\right)\right], \tag{3}$$

where k_{Brown} is a kinetic constant with units of inverse time, representing Brownian, structure restoration effects and t_{r1}, t_{r2} are two thixotropic constants, connected to the breaking and aggregation kinetic constants k_{Break} and k_{Aggr}

$$\hat{t}_{r1} = \left(\frac{k_{\text{Break}}}{k_{\text{Brown}}}\right)^{1/a} \tag{4}$$

$$\hat{t}_{r2} = \left(\frac{k_{\text{Aggr}}}{k_{\text{Brown}}}\right)^{1/d} \tag{5}$$

In the original "structural kinetics model for thixotropy" [1] a similar format was used for the structure evolution equation with the addition of a time-dependent prefactor, which makes the model inappropriate for LAOS as it depends on absolute time and will not reach an alternance state. Additionally, we allow for variable exponents a and d, while Dullaert and Mewis [3] use explicit values of 1 and 0.5, respectively. Importantly, the MDTM incorporates aspects from the work of Dimitriou *et al.* [37], who developed a framework to separate strain and shear rate into elastic and plastic components [37] to better capture the EVP behavior of soft solid materials. In particular, according to the theory of kinematic hardening of plasticity, [37], the strain and shear rate each have elastic and viscous components, and together the components add up to the total strain and shear rate, respectively,

$$\gamma = \gamma_e + \gamma_p \leftrightarrow \dot{\gamma} = \dot{\gamma}_e + \dot{\gamma}_p. \tag{6}$$

In turn, the elastic strain, γ_e is postulated to evolve as [6]

$$\dot{\gamma}_e = \dot{\gamma}_p - \frac{\gamma_e}{\gamma_{\max}}|\dot{\gamma}_p|. \tag{7}$$

This adds an equation for the MDTM modulus,

$$\frac{dG_f}{dt} = -k_G(G_f - \lambda G_0), \tag{8}$$

which imparts an additional time constant $\propto k_G^{-1}$ for this process. In the original structural kinetics model for thixotropy Dullaert and Mewis [3] used an algebraic equation for variable elastic modulus, $\lambda G_0\gamma_e$ at each shear rate, where G_0 is the fully structured elastic modulus, λ is the current structure level, and γ_e is the elastic strain. In the Dullaert and Mewis structural kinetics model for thixotropy, the elastic strain is an ordinary differential equation (ODE), and a more detailed description is provided in literature [3].

Our model differs from that of Dimitriou *et al.* [37] in the following ways:

- The MDTM uses an ordinary differential equation to evolve the elastic modulus in time, with k_G, an elastic modulus time constant.
- The MDTM incorporates a unique ordinary differential equation for elastic strain, γ_e, that is a function of the

Redistribution subject to SOR license or copyright; see http://scitation.aip.org/content/sor/journal/jor2/info/about. Downloaded to IP: 128.175.82.78 On: Fri, 01 Apr 2016 15:11:45

current plastic strain, γ_p, in such a way that the sum of plastic and elastic strain is always equal to total strain.
- The MDTM incorporates an ordinary differential equation for the structural evolution that involves a term for shear aggregation.
- The maximum strain, $\gamma_{\max}$, is set as a limit to ensure that the material cannot accumulate more strain than the material limit.

In the model, strain is the linear superposition of an elastic strain and a plastic strain, with shear rate correspondingly the linear superposition of elastic shear rate and plastic shear rate, as shown in Eq. (6). The calculation of the plastic component of shear rate is

$$\dot{\gamma}_p = \begin{cases} \dfrac{\dot{\gamma}}{\left(2 - \dfrac{|\gamma_e|}{\gamma_{\max}}\right)} & \dot{\gamma} \geq 0 \\ \dfrac{\dot{\gamma}}{\left(2 + \dfrac{|\gamma_e|}{\gamma_{\max}}\right)} & \dot{\gamma} < 0 \end{cases} \tag{9}$$

and is a function of shear rate, $\dot{\gamma}$, elastic strain, γ_e, and maximum strain, $\gamma_{\max}$, where $\gamma_{\max}$ represents the maximum elastic strain the material can withstand, and is postulated to be a function of the structure parameter as

$$\gamma_{\max}(\lambda) = \min\left(\frac{\gamma_{CO}}{\lambda^m}, \gamma_\infty\right) \tag{10}$$

Note that this expression requires the following connectivity at the zero deformation limit between the yield stress, σ_{y0}, and the zero deformation strain, γ_{CO} appearing in Eq. (10) above

$$\gamma_{CO} = \frac{\sigma_{y0}}{G_0}. \tag{11}$$

With this understanding it is now possible to cast the constitutive equation as a sum of elastic and plastic components, where the elastic components are aligned with stretching, reversible processes, and the plastic components are aligned with irreversible, dissipative processes. An earlier version of this thixotropy model has recently been applied to successfully model and predict blood flow [4]. The stress decomposition within MDTM has an additional viscous stress term, namely the structural viscosity

$$\sigma = G_f\gamma_e + \lambda K_{ST}\dot{\gamma}_p^{n_2} + K_\infty\dot{\gamma}_p^{n_1}, \tag{12}$$

where the first term represents elastic stress, and the second and third terms represent structural, and solvent contributions to the viscous stress with consistency parameters, K_{ST}, K_∞ and analogous power law parameters n_2 and n_1.

As presented, there are 14 parameters in the MDTM. However, γ_∞ in Eq. (10) is empirically set to be 1 in this work. We find, however, that under no circumstances is λ sufficiently small such that the maximum elastic strain reaches this value; however, we include it in the model description for completeness. Consequently, we can drop this parameter and limit from consideration for what follows. We also note that, as written, the stress given in Eq. (12) violates thermodynamic consistency in that upon flow cessation from steady shear, both the plastic [Eq. (9)] and elastic [Eq. (7)] strain rates immediately go to zero. As the structure rebuilds upon flow cessation via Brownian motion, the modulus will also increase [see Eq. (8)] such that the elastic stress will also increase upon flow cessation. This anomalous effect is common among thixotropy models (see [8]) and can be corrected by including an additional relaxation term in Eq. (7) such that the elastic strain can relax to zero upon flow cessation.

There are 13 parameters to determine in the MDTM, which are tabulated, along with their units, best-fit values and uncertainties in Table I. The determination of these model parameters from experimental data is discussed further in Sec. III B.

B. Literature models

The additional models from literature that were examined herein are briefly discussed in the Supplementary Material [44], with their respective equations listed, and primary source

TABLE I. Parameter values determined for the MDTM. The five shaded parameters are fit to specific aspects of the experimental data while the remaining eight parameters are determined by global fitting of the steady and transient data.

Parameter	Units	Meaning	Range initial guess	Limiting values	Optimal	Average	Range: (±)
σ_{y0}	Pa	Yield stress	(-)	(-)	11	(-)	(-)
η_∞	Pa s^{n1}	Infinite shear viscosity	(-)	(-)	1.17	(-)	(-)
n_1	(-)	Power law exponent K_∞	(-)	(-)	1	(-)	(-)
G_0	Pa	Elastic modulus	(-)	(-)	450	(-)	(-)
m	(-)	Power law exponent of γ_e evolution	(-)	(-)	−1.5	(-)	(-)
K_{ST}	Pa s^{n2}	Consistency parameter	[9–11]	>0	11.21	11.36	0.547
n_2	(-)	Power law exponent K_{ST}	[0.5–1]	[0.5–1]	0.81	0.82	0.019
a	(-)	Power law exponent for shear breakage	[1–2]	[1–2]	1.53	1.51	0.036
d	(-)	Power law exponent for shear aggregation	[0.25–0.75]	[0.25–0.75]	0.65	0.59	0.05
k_{Brown}	s^{-1}	Characteristic time of Brownian motion	$[1 \times 10^{-3}$–1]	>0	0.28	0.28	0.041
$\hat{t}_{r1}$ (k_{Break}/k_{Brown})	s	Characteristic time of λ shear breakdown	$[1 \times 10^{-3}$–1]	>0	0.77	0.81	0.23
$\hat{t}_{r2}$ (k_{Aggr}/k_{Brown})	s	Characteristic time of λ shear buildup	$[1 \times 10^{-3}$–1]	>0	2.0	2.76	0.17
k_G	s^{-1}	Characteristic time of G evolution	$[1 \times 10^{-3}$–1]	>0	0.09	0.09	0.024

Redistribution subject to SOR license or copyright; see http://scitation.aip.org/content/sor/journal/jor2/info/about. Downloaded to IP: 128.175.82.78 On: Fri, 01 Apr 2016 15:11:45

as well, in order of increasing complexity, from the simplest to the most complicated. The simple scalar thixotropic model (SST) equations are Eqs. (S.1)–(S.3) [9]. The unified approach model (UA) equations are Eqs. (S.4)–(S.14) [7]. The BMP equations are Eqs. (S.15) and (S.16) [6].

III. MATERIALS AND METHODS

A. Thixotropic suspension

The model thixotropic suspension reported by Dullaert and Mewis [4] was reformulated for this work, following as closely as possible the prescribed methods. The suspension consists of 2.9 vol. % fumed silica (Evonik Aerosil® R972) aggregates with primary particle radius of 16 nm in a blend of 69 wt. % paraffin oil, (Sigma Aldrich, density 0.827–0.890 g/cc) and 31 wt. % poly-isobutylene (TPC Group, molecular mass 750(g/mol)). Note that the polyisobutylene (PIB) molecular mass differs from that of the polyisobuylene used by Dullaert and Mewis [3,4] due to availability. The particles as supplied are imaged with transmission electron microscopy and shown in Fig. 1, where it is apparent that the nominally 16 nm primary particles are aggregated into large, (micron) sized agglomerates. The particles were dispersed in the blended solution using a Silverson Mixer, model L4Rt using the tubular mixing unit with square hole high shear screen at the 8000 rpm setting for 30 min. This was followed by degassing at 40 °C in a vacuum chamber for 1 h. Samples were stored under gentle rolling conditions on a Wheaton benchtop roll-mixer.

Figure 2(a) compares the steady shear viscosity with that reported by Dullaert and Mewis [3,4]. The data superimpose well, where differences are attributed primarily to the difference in the background viscosity of the suspending fluid blend (0.39 $_{\text{Pa s}}$ as compared to 0.65 $_{\text{Pa s}}$) reported by Dullaert and Mewis [3,4]. Superimposed on the plot are the error bars calculated from four different experiments using the t-distribution with 95% confidence interval [57]. The difference evident at high shear rates arises from differences in the solvent viscosity and that the two colloidal suspensions are not identical—the system of Dullaert and Mewis [3,4] has larger aggregates (>1 μm). Differences in particle agglomerate size will also affect the elastic stresses, as seen in Fig. 2(a). Our results are in semiquantitative agreement with the prior work and the similarities enable direct comparisons between the two data sets.

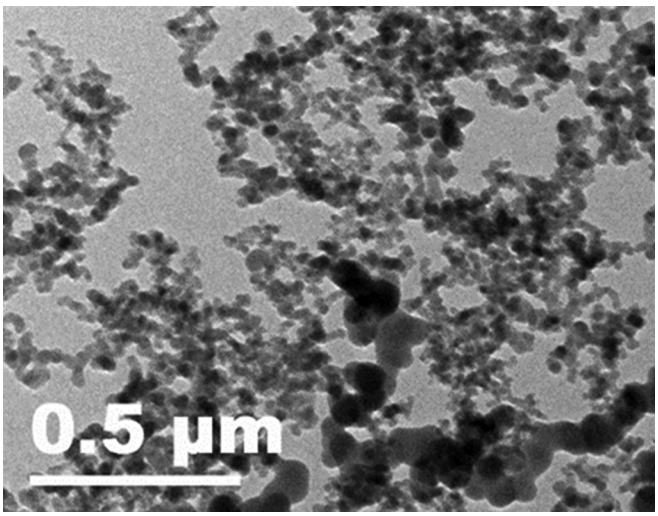

FIG. 1. Transmission electron microscope micrograph of the fumed silica (Degussa R972) aggregates as supplied (courtesy of Ryan Murphy, University of Delaware).

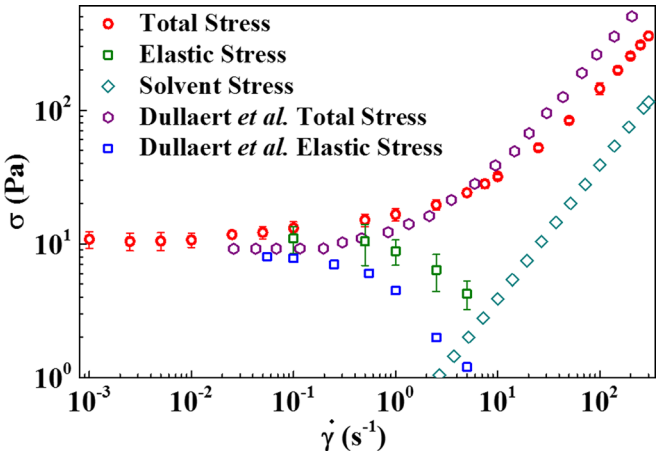

FIG. 2. (a) Steady state flow curve experimental results of model thixotropic system (2.9 vol. % fumed silica in paraffin oil and PIB), compared against the results of Dullaert and Mewis [1,2] and the solvent mixture. Also shown are the contributions from the elastic stress as obtained from stress jumps, with the error bars, compared against the results from Dullaert and Mewis [2,57].

B. Rheological measurement protocol

Rheological measurements were performed with an ARES G2, strain controlled rheometer (TA Instruments) using a 50 mm cone and plate geometry with 0.0404 rad cone angle Dynamic yield stress experiments were conducted on a DHR3 stress controlled rheometer (TA Instruments) with 40 mm cone and plate geometry with a 0.04 rad cone angle. Measurements of the stress at each shear rate in the steady flow curves were performed after a preshear of 300 s^{-1} for 300 s. Following the completion of each preshear the new shear rate was set and allowed to equilibrate for a varying amount of time depending on the shear rate. For the highest shear rate (300 s^{-1}) this time was determined to be 10 min. For the lowest shear rate [10^{-3} (s^{-1})] this time was determined to be 2 h. Equilibration times were determined by requiring the time derivative of the stress to effectively reach zero. All of the transient step-up and step-down series were preceded by a preshear of 300 s^{-1} for 300 s, followed by a period of time to arrive at a steady stress value for a given initial shear rate (600–900 s for all shear rates). The LAOS flows were preceded by a preshear of 300 s^{-1} for 300 s in the same manner. Some of the LAOS experiments started from a fully structured state, which required a rest period (or soak time) of 10 min, but the results presented here are for the alternance state, which is independent of the initial state. Values of the viscosity obtained during the preshear were used before and after each experiment to determine that no irreversible changes occurred to the sample during testing. The rheological data presented here were found to be

Redistribution subject to SOR license or copyright; see http://scitation.aip.org/content/sor/journal/jor2/info/about. Downloaded to IP: 128.175.82.78 On: Fri, 01 Apr 2016 15:11:45

reproducible from loading to loading and batch to batch of sample.

The elastic stress was measured using a strain jump experiment following the procedure outlined by Dullaert and Mewis and is shown in the Supplementary Material [44,58], Fig. S.1(b). This experiment rapidly reduces the shear rate from a steady, constant value to a value near zero at prescribed time. The viscous forces go to zero with the shear rate [9,59] such that extrapolation of the residual stress back to the time of the rate reduction yields a measure of the elastic component of the total stress derived from the rheometer's torque measurement.

C. MDTM parameter determination procedure

The thirteen parameters of the MDTM are listed in Table I. The parameters are listed generally in the order they were determined, which can be characterized as a two-step process. The first five parameters listed in Table I were fit to specific aspects of the experimental data as follows: the first three parameters $\sigma_{y0}, \eta_\infty, n_1$, are determined using the steady state flow curve and its limiting values at the shear rate extremes, while G_0 and m are evaluated with the SAOS data, steady flow curve, and the critical relationship $\gamma_{CO} = \sigma_{y0}/G_0$. At the end, the value for the critical yield stress is corroborated with the G'–G'' crossover amplitude shown in Fig. S.2 (Supplementary Material [44]). The critical strain γ_{CO} was shown to compare well with the strain at the limit of linearity as determined from selected amplitude sweep experiments shown in the Supplementary Material [44], Fig. S.2. All of the other parameters are then determined simultaneously with the parallel simulated annealing algorithm, while keeping the first 5 parameters constant $(\sigma_{y0}, \eta_\infty, n_1, G_0, \mathrm{m})$ during this process.

To fit the remaining eight parameters to the experimental data we define an objective function to be minimized F_{OBJ}, which is a summation of the L_2 norm applied to each respective data set, shown in Eq. (13), divided by number of points, P, in each dataset. F_{OBJ} is the sum of the relative errors of each respective data set divided by the total number of data sets, M [56],

$$F_{OBJ} = \frac{1}{M}\sum_{k=1}^{N}\frac{1}{P_k}\left\|\frac{(\sigma_{Model}-\sigma_{Data})}{\sigma_{Data}}\right\|_{2,k}. \qquad (13)$$

The experimental data used during this nonlinear dynamic parameter fitting were the steady state flow curve [Fig. 3(a)], the elastic stresses, [Fig. 3(a)] and the sixteen sets of transient step-up and step-down data [see Figs. 4(a)–4(d) as examples]. In the global fitting, constraints were imposed on some parameters. The range used for the a, and d values has been discussed in literature for a thixotropic material, where a has been recommended to range between one and two, [3,4,9] while it has been suggested [3], that the value of d be set close to $1/2$, such that the range 0.25–0.75 is feasible. Additionally, as the material is shear thinning, we constrained n_2 to lie between 0.5 and 1 [9]. Importantly, the final fit values were not limited by the extremes of these ranges.

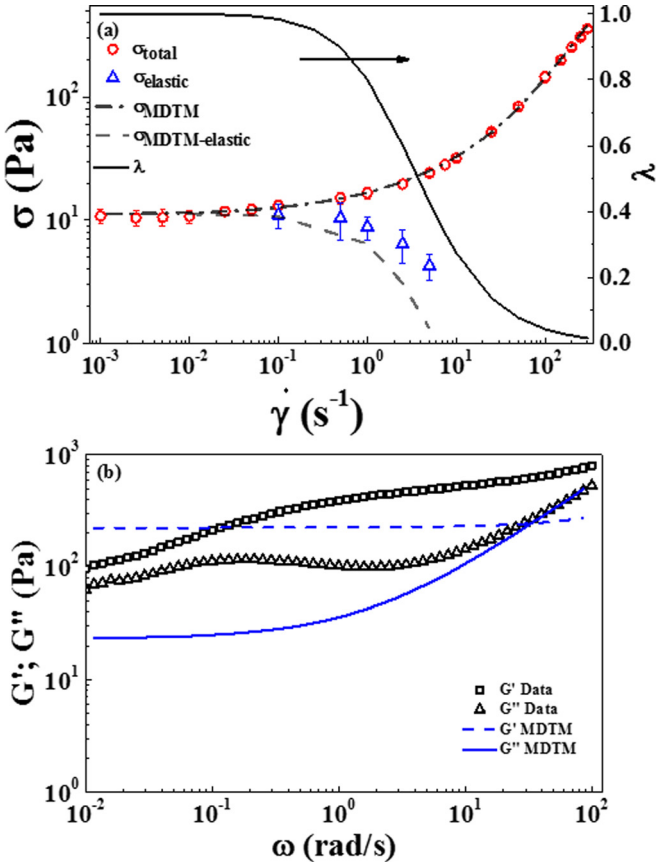

FIG. 3. (a) Steady state flow curve of model thixotropic system with MDTM fit and λ and (b) small amplitude oscillatory shear (frequency sweep, $\gamma_0 = 0.01$) results with MDTM best fit.

From the results of the 15 trials, statistics were calculated, including parameter averages, and standard deviations. This is detailed in Table I, and the values of the 15 trials for each parameter are shown in Table S.1. The parameter values giving the smallest value of F_{OBJ} defined in Eq. (13) were used for the results presented in this work (Table I), which are presented along with the average and standard deviation of the 15 independent fits. The MDTM always converged to a single basin with respect to F_{OBJ} as observed from the parameter values from the 15 trials. The parameter correlation matrix is shown in Table S.3 along with an analysis.

IV. EXPERIMENTAL RESULTS AND MODEL COMPARISONS

A. Experimental results and MDTM comparisons

A comparison of the steady state flow curve and elastic stresses with the best fit of the MDTM, over more than 5 orders of magnitude variation in shear rate is shown in Fig. 3(a). The data exhibit a distinct yield stress at low shear rates and shear thinning at moderate values of shear rate and transitions to a nearly constant high shear viscosity at rates in excess of $100\,\mathrm{s}^{-1}$. To help interpret the data, the model predictions for the structure parameter λ are also shown. The structure parameter is close to 1 (corresponding to a fully structured material) until the stress rises significantly above

Redistribution subject to SOR license or copyright; see http://scitation.aip.org/content/sor/journal/jor2/info/about. Downloaded to IP: 128.175.82.78 On: Fri, 01 Apr 2016 15:11:45

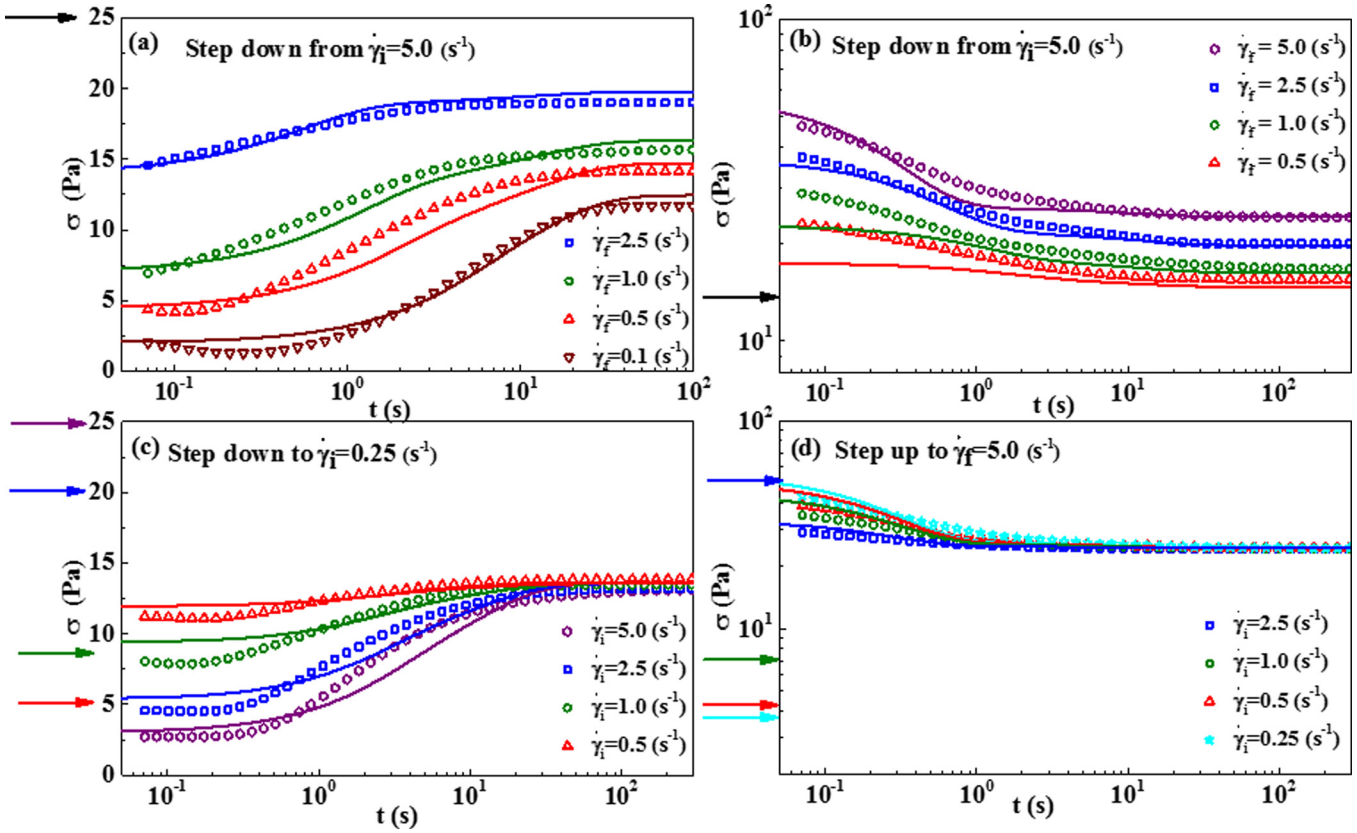

FIG. 4. (a) Data and MDTM fits of step down in shear rate from 5.0 s^{-1} to 4 different values as indicated; (b) data and fits of step up in shear rate from 0.1 s^{-1} to 4 different values; (c) data and fits of step down to 0.25 s^{-1} from 4 different values (in this data the initial shear rates are the same while the final shear rates vary); and (d) data and fits of step up to 5.0 s^{-1} from 4 different values as indicated in plot (in this data the final shear rates are the same while the initial shear rates vary). The arrows indicate the stress starting values before the step up or step down in shear rate.

the yield stress, whereupon it decreases to become fully unstructured ($\lambda = 0$) at the highest shear rates probed. The elastic component of this steady shear stress is observed to decrease as the structure is broken down by the flow. The MDTM predicts this effect, but at slightly lower shear rates than observed experimentally.

The small amplitude oscillatory shear measurements over 4 orders of magnitude of frequency are shown in Fig. 3(b). The experimental spectrum does not exhibit a terminal liquid regime at the lowest frequencies probed, but rather, is characteristic of a material with an apparent yield stress. The small amplitude oscillatory shear frequency sweep is fit to a spectrum of five relaxation times, each with a corresponding modulus, to yield the relaxation spectrum, as shown in Supplementary Material [44], Table S.8, over the range [0.001–∞]. These data also suggest that any terminal relaxation process to a thixotropic liquid must be on the order of at least 1000 s. The amplitude sweep experiments used to define the linear regime are shown in the Supplementary Material [44] [Figs. S.2(a) and S.2(b)]. Importantly, the model calculations are performed at the same frequency and strain amplitude (1%) used in the experiment. The amplitude sweeps verify that, up to frequencies of order 10 rad/s, this amplitude is sufficient to be in the linear regime. Indeed the structure parameter is ∼1 even at the highest frequencies probed for this amplitude, which corresponds to a shear rate amplitude of 1 s^{-1}. Empirically, it is observed that this material in a sealed bottle left on the shelf will creep over the course of many days, demonstrating that thixotropic relaxation processes are more extended than the viscoelastic relaxation process that consists of a recoil process.

Fits to the MDTM are also shown in Fig. 3(b), where the zero frequency limit of the elastic modulus is 225 Pa [dashed line in Fig. 3(b)]. To make this determination, both the SAOS frequency sweep and amplitude sweep were used to simultaneously determine the low frequency plateau of the frequency sweep and the y-intercept at the small strain amplitude extreme of the amplitude sweep data. A value for the critical yield strain γ_{CO} is calculated from the ratio of the yield stress and elastic modulus [Eq. (11)] to be 0.024. This agrees well with the values identified in the strain sweep experiments (see Fig. S.2 in Supplementary Material [44]), providing confidence in these parameter values. Note that the MDTM has a frequency-independent elastic modulus due to the separation of strain into plastic and elastic terms, which yields both elastic and viscous contributions to the equilibrium moduli. The loss modulus has a contribution from the viscous stresses, which becomes evident at higher frequencies. The MDTM best fits are also shown, where the model's simple representation of the elastic yield stress leads to an elastic modulus, G′ that does not depend on frequency, and hence, can only approximately represent the experimentally observed spectrum.

Two basic protocols are followed for the step up and step down in shear rate experiments. The first is transitioning to a common final shear rate from different values of initial,

Redistribution subject to SOR license or copyright; see http://scitation.aip.org/content/sor/journal/jor2/info/about. Downloaded to IP: 128.175.82.78 On: Fri, 01 Apr 2016 15:11:45

steady shear rate. The second protocol consists of transitioning from a common initial rate to different final values of shear rate. The results of the step up and step down experiments are shown in Figs. 4(a)–4(d), where the initial stress values, as indicated by the arrows, correspond to points on the steady flow curve [Fig. 3(a)] and only the transient stress responses from the time of the rate jump are shown in the figure so they can be presented on a logarithmic time scale for clarity. These results follow trends characteristic of a thixotropic material and closely follow the observations of Dullaert and Mewis [3]. Comparison of these curves shows that there are different time scales for structure break down and build up, and that these processes depend on the rate of deformation. Furthermore, there are vestigial elastic signatures at early times showing that the material is not purely thixotropic in its response.

Structure predictions from the MDTM are shown in Figs. 5(a)–5(d) corresponding to Figs. 4(a)–4(d). Using the steady state flow curves for reference [Fig. 3(a)], the MDTM predictions for structure evolution during these transient tests can be interpreted. Namely, structure rebuilds upon lowering the applied shear rate, leading to an increase of the viscosity and yield stress. An increase of the shear rate results in the opposite process. Furthermore, the structure evolution is monotonic during these processes, explaining the monotonic behavior of the model predictions for shear stress. We also find that the shear induced breakage and aggregation terms are dominant at finite shear rates, which supports the inclusion of a shear aggregation term in the structure kinetics equation. Because these two shear-dependent processes have a different power law index, there is no simple reduction of this transient behavior to a uniform master curve, as observed for the simpler SSTM (see Mewis and Wagner [9], Chap. 7).

B. Comparison to literature models

In addition to the MDTM, three thixotropy models from the literature have been used to fit the data: The SST model [9]; the UA model [7]; and BMPM [8]. In this section we highlight some key comparisons of the four model fits to the experimental data sets presented in Secs. III A and III C, as well as Sec. IV A. Detailed comparisons of the best fits for each of the three models, presented in the same level of detail as for the MDTM, can be found in the Supplementary Material [44].

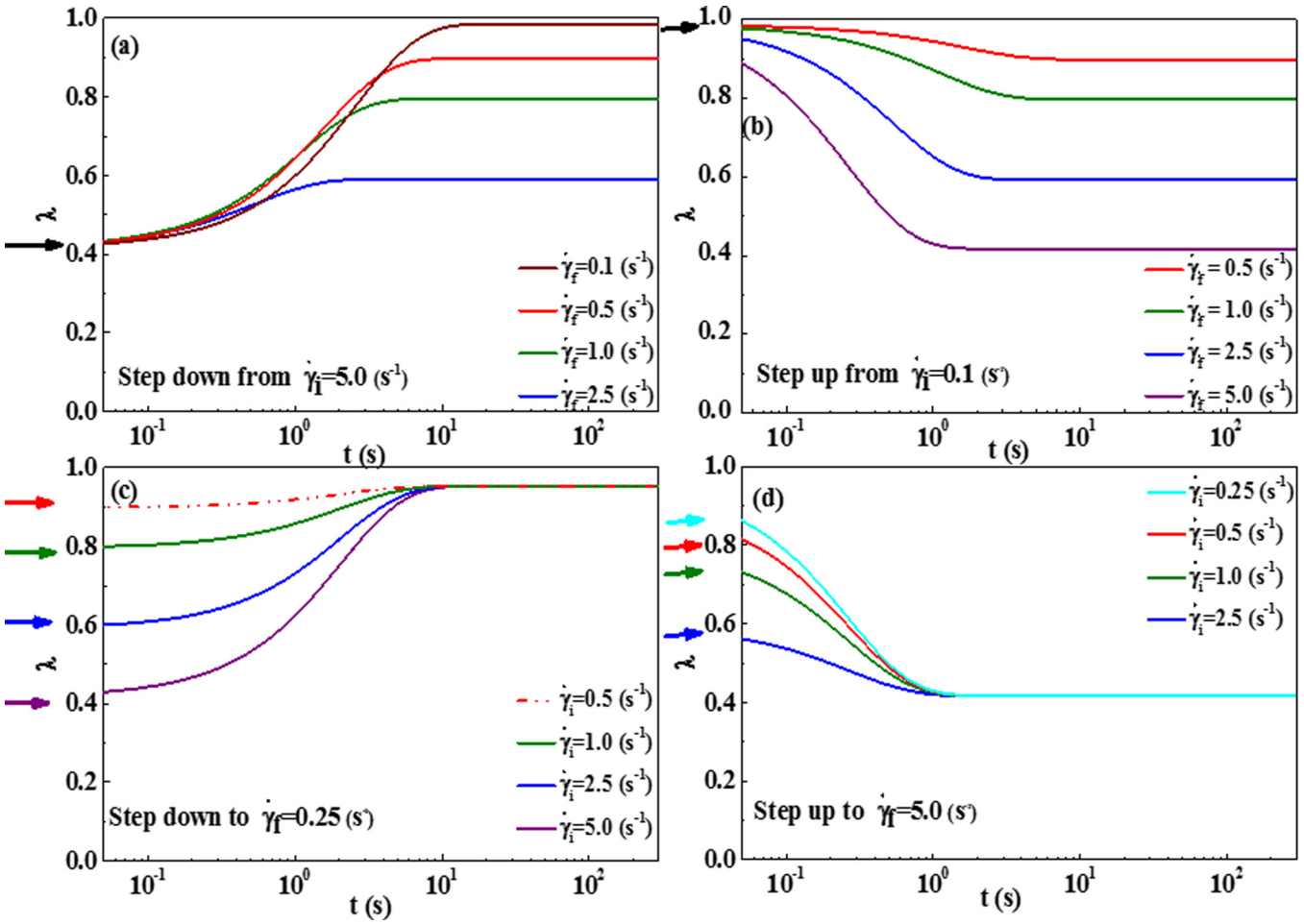

FIG. 5. (a) MDTM Structure predictions of step down in shear rate from 5.0 s^{-1} to 4 different values as indicated; (b) structure predictions of step up in shear rate from 0.1 s^{-1} to 4 different values as indicated; (c) structure predictions of step down to 0.25 s^{-1} from 4 different values as indicated (in this data the initial shear rates are the same while the final shear rates vary); (d) structure predictions of step up to 5.0 s^{-1} from 4 different values as indicated (in this data the final shear rates are the same while the initial shear rates vary); All predictions are calculated with the parameter values in Table I. The arrows indicate the structure (λ) starting values before the step up or step down in shear rate.

Redistribution subject to SOR license or copyright; see http://scitation.aip.org/content/sor/journal/jor2/info/about. Downloaded to IP: 128.175.82.78 On: Fri, 01 Apr 2016 15:11:45

The steady state flow curves are compared with model predictions for each of the four models in Fig. 6(a). Not surprisingly, all of the models have more than enough parameters to accurately model the steady state flow curve (SSTM: 5 parameters; MDTM: 13 parameters; UAM: 10 parameters; BMPM: 30 parameters—five relaxation modes). Figure 6(b) shows that the SSTM, and UAM fail consistently to approximate the SAOS spectrum, whereas the multimode BMPM, with its 30 parameters can very accurately fit the linear viscoelastic material response (by construction). The MDTM predictions fall somewhere between these two limits. Previous work has identified that elasticity in aggregated or flocculated suspensions can arise from both intra and inter aggregate interactions [60]. The simplified expressions for the yield stress employed in single scalar parameter structural thixotropy models can only capture the overall behavior qualitatively at best (as shown here for the MDTM) and not the detailed frequency dependence of the moduli. However, as the focus of thixotropy models is the time dependent flow behavior under nonlinear conditions, the level of approximation afforded by the MDTM is sufficient and qualitatively similar to that of the SSTM and the UAM.

Examination of the step-down and step-up in shear rate results and model fits in Figs. 7(a) and 7(b) shows significant

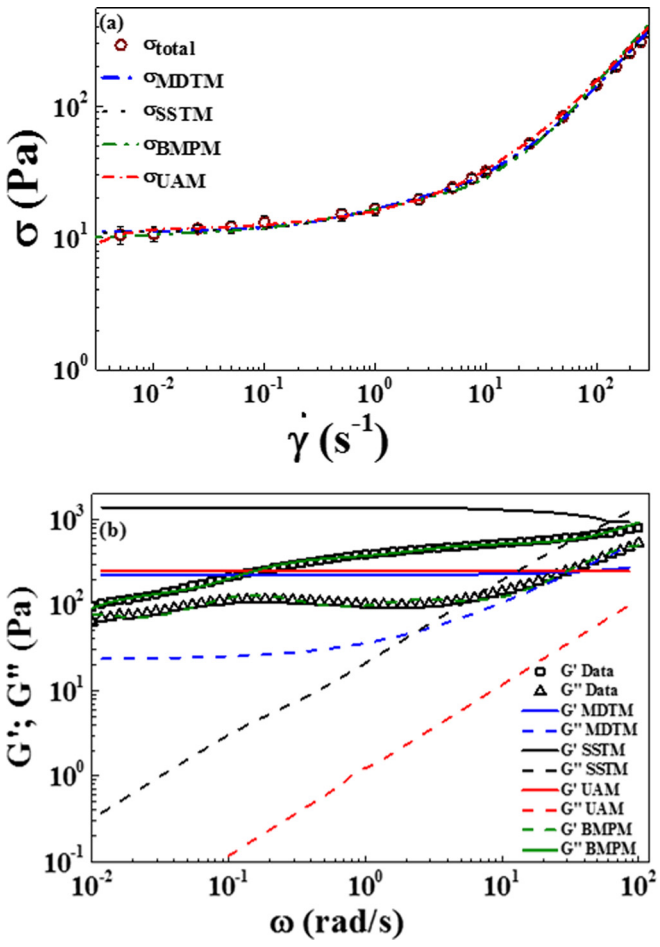

FIG. 6. (a) Steady state flow curve model fits and data for all four models and (b) small amplitude oscillatory shear predictions and data for all four models.

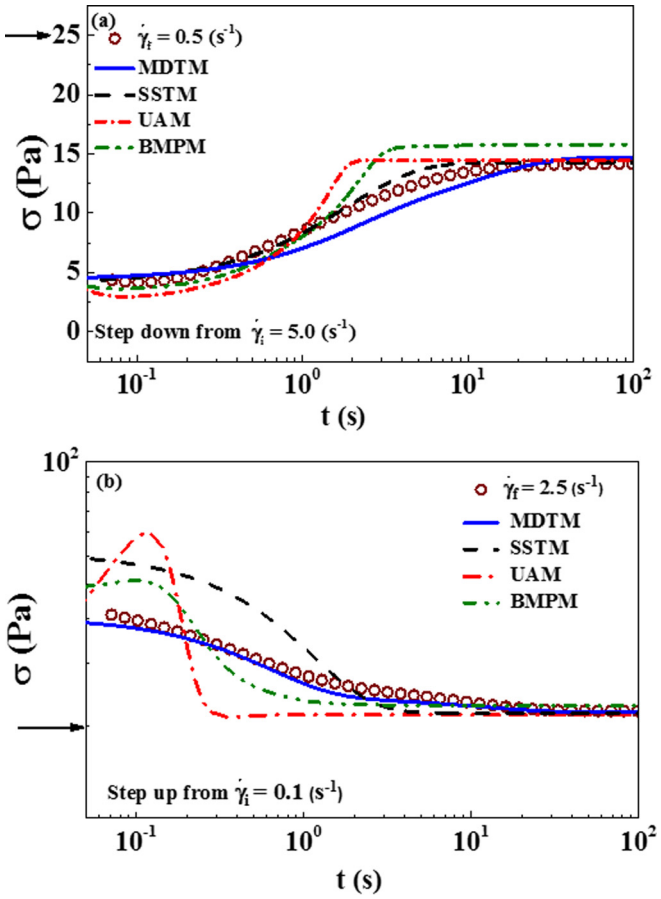

FIG. 7. (a) Single step-down in shear rate from 5.0 to 0.5 s^{-1} and data comparison with all four models and (b) single step-up in shear rate from 0.1 to 2.5 s^{-1} and data comparison with all four models.

differences between the models (note only two characteristic curves are provided here for brevity and the rest are presented in the Supplementary Material [44]). The MDTM can fit the data well, while the SST model is less satisfactory from a quantitative perspective and both the UA and BMPM approach yield qualitative inconsistencies. The advantages of the MDTM over the SSTM is also due to the addition of a third process to account for shear-induced aggregation, which is important for accurately modeling the differences in recovery processes between increases and decreases in shear rate. In contrast, the UAM and BMPM include processes that always lead to both viscoelastic and thixotropic responses in rate jump experiments. These viscoelastic processes are also clearly evident in some of the other comparisons shown in the Supplementary Material [44]. This is especially true for the five-mode BMPM, which is constructed on a viscoelastic framework. However, these additional viscoelastic short time transients are not observed in the data.

What is apparent from these comparisons is that accurate constitutive models for nearly ideal thixotropic materials under time dependent nonlinear shear flow require a dominant viscous response that is coupled to a time and rate dependent structure. Although viscoelastic models can capture some aspects of nearly ideal thixotropic systems, they fail to capture the dominant qualitative features inherent in thixotropic flows.

Redistribution subject to SOR license or copyright; see http://scitation.aip.org/content/sor/journal/jor2/info/about. Downloaded to IP: 128.175.82.78 On: Fri, 01 Apr 2016 15:11:45

However, fits to already known data can be deceptive. In Sec. V, we compare *predictions* of these models obtained with the same fit parameters against various additional time-dependent flows that are used for characterizing thixotropic materials.

V. PREDICTING STRESS RESPONSE UNDER NONLINEAR, TRANSIENT SHEAR FLOWS

A. Large amplitude oscillatory shear

LAOS experimental results are presented in Figs. 8(a)–8(d) for a range of frequencies and strain amplitudes, shown in dimensionless form for ease of comparison. Inspection reveals characteristics of both thixotropic and viscoelastic behavior; for example, in Fig. 8(a), in the $\omega = 0.01(\mathrm{rad/s})$ data, a yielding behavior can be clearly observed (seen in the shoulder, indicating yielding). In addition, at the higher strain amplitudes there is clear evidence of stress overshoots leading to secondary LAOS loops in the viscous projections. This indicates that there is structure reforming and breaking down during this portion of the LAOS cycle. This is a consequence of a lag time within the structured material such that the structure breakdown lags behind the instantaneous shear rate, so called "thixotropic loops" in classical thixotropic tests (e.g., see Chap. 7, Mewis and Wagner [9]). This effect becomes less evident as the frequency is increased from 0.01 to 10 (rad/s), whereupon the sample exhibits a predominantly viscous stress response. This is expected as $\dot{\gamma}_0$ is increasing, which leads to less structure, and consequently, more viscous behavior. It is the structure that directly contributes to the elastic nature of the material, and if the frequency is sufficiently high, the structure cannot recover sufficiently during the cycle time. A similar interpretation has also made by de Souza Mendes *et al.* [61]. Furthermore, direct observation of this effect has been made for colloidal gels by Kim *et al.* [28], where measurements of the structure under flow verified this interpretation.

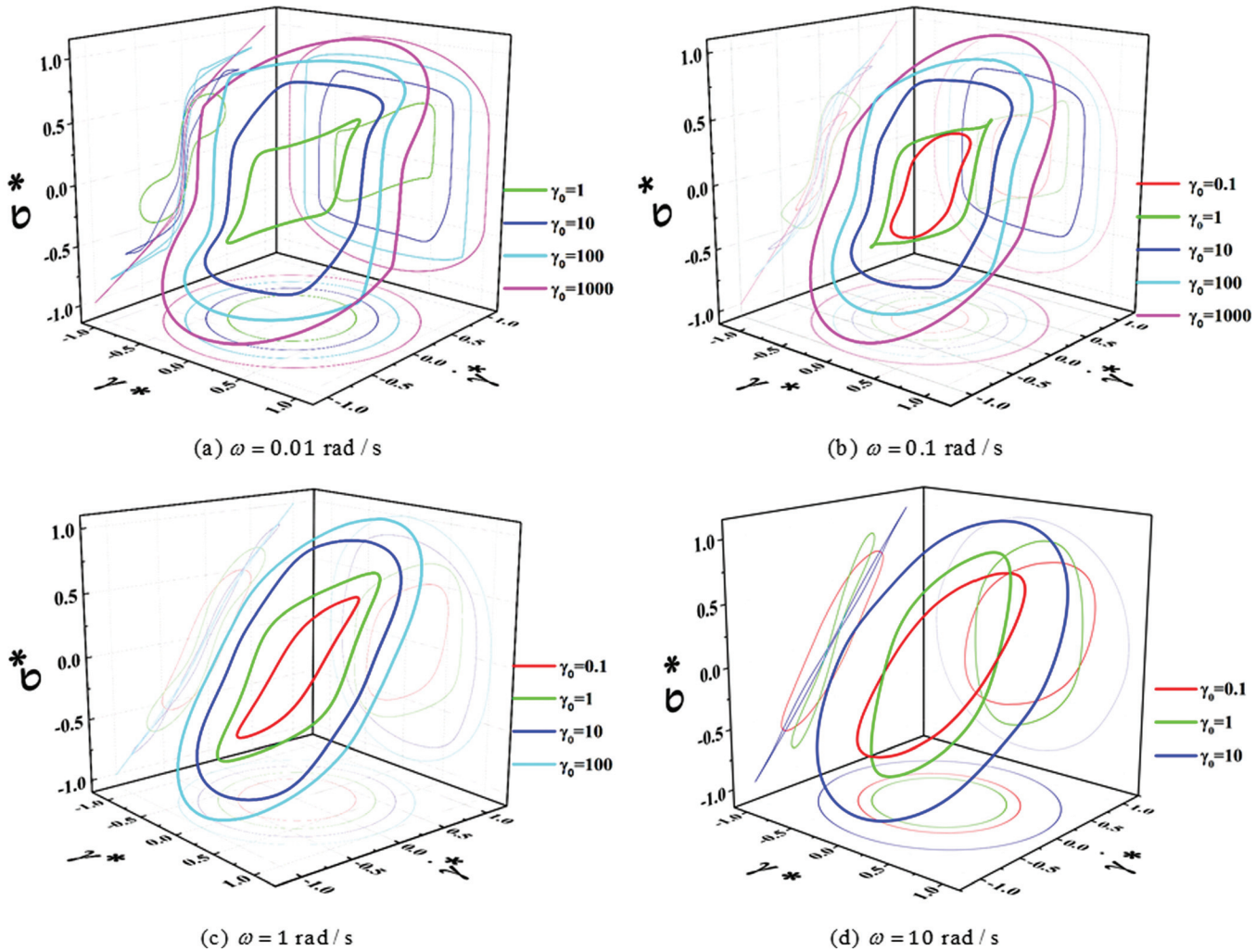

FIG. 8. (a) LAOS data at $\omega = 0.01$ (rad/s) over a range of strain amplitudes (LAOS data normalized by maximum values, then normalized stress values scaled by 0.5, 0.67, 0.83, and 1 for $\gamma_0 = 1, 10, 100,$ and1000, respectively, for presentation purposes). (b) LAOS data at $\omega = 0.1$ (rad/s) over a range of γ_0 (LAOS data normalized by maximum values, then normalized stress values scaled by 0.33, 0.5, 0.67, 0.83, and 1 for $\gamma_0 = 0.1, 1, 10, 100,$ and1000, respectively, for presentation purposes). (c) LAOS data at $\omega = 1$ (rad/s) over range of γ_0 (LAOS data normalized by maximum values, then normalized stress values scaled by 0.5, 0.67, 0.83, and 1 for $\gamma_0 = 0.1, 1, 10,$ and100, respectively, for presentation purposes). (d) LAOS data at $\omega = 10$ (rad/s) over range of γ_0 (LAOS data normalized by maximum values, then normalized stress values scaled by 0.67, 0.83, and 1 for $\gamma_0 = 0.1, 1,$ and10, respectively, for presentation purposes).

Redistribution subject to SOR license or copyright; see http://scitation.aip.org/content/sor/journal/jor2/info/about. Downloaded to IP: 128.175.82.78 On: Fri, 01 Apr 2016 15:11:45

Model predictions are performed by simulating LAOS for a sufficient number of cycles until alternance is achieved, in a manner similar to the experiments. In this context, alternance refers to the state of LAOS whereby the stress and structure, although continuously evolving over a period, do so such that stress and structure repeat over consecutive periods. Comparisons are made in both elastic and viscous projections, with the respect to $\gamma(t)$, and, respectively, $\dot{\gamma}(t)$, of the Lissajous–Bowditch figures. To illustrate a typical model behavior, we show the three dimensional Lissajous–Bowditch plot comparing the experimental data with predictions of the MDTM at $\omega = 1\text{rad/s}$; $\gamma_0 = 10$ at, and $\omega = 1\text{rad/s}$; $\gamma_0 = 1$ in Figs. 9(a)–9(e), and 10(a)–10(e), respectively.

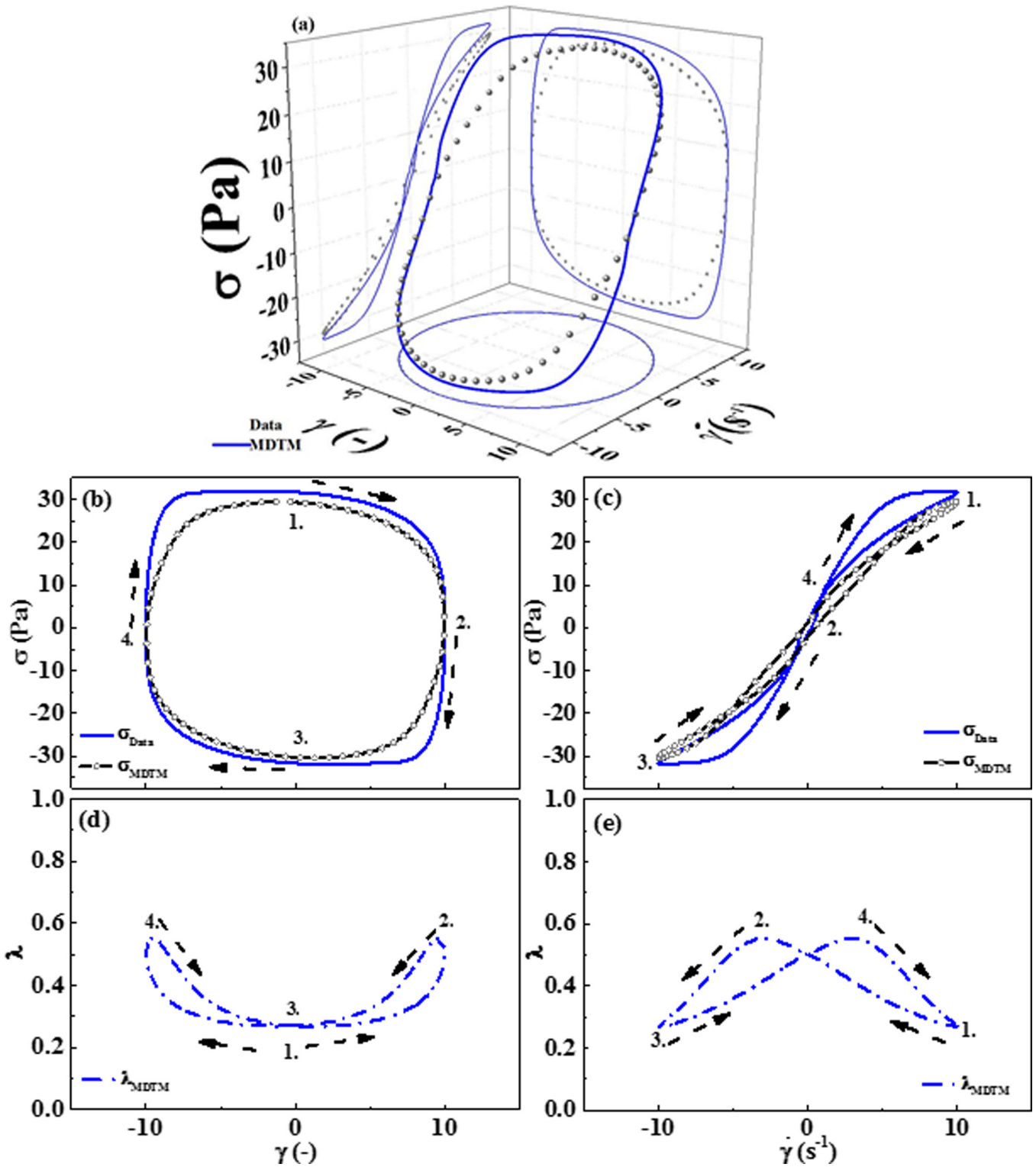

FIG. 9. (a) Three dimensional Lissajous–Bowditch curve for $\omega = 1\text{rad/s}$; $\gamma_0 = 10$; (b) two dimensional elastic projection; (c) two dimensional viscous projection; (d) two dimensional structural, elastic projection; (e) two dimensional structural viscous projection. The arrows indicate the direction of time evolution during the cycle and the numbers correspond to specific states discussed in the text.

Redistribution subject to SOR license or copyright; see http://scitation.aip.org/content/sor/journal/jor2/info/about. Downloaded to IP: 128.175.82.78 On: Fri, 01 Apr 2016 15:11:45

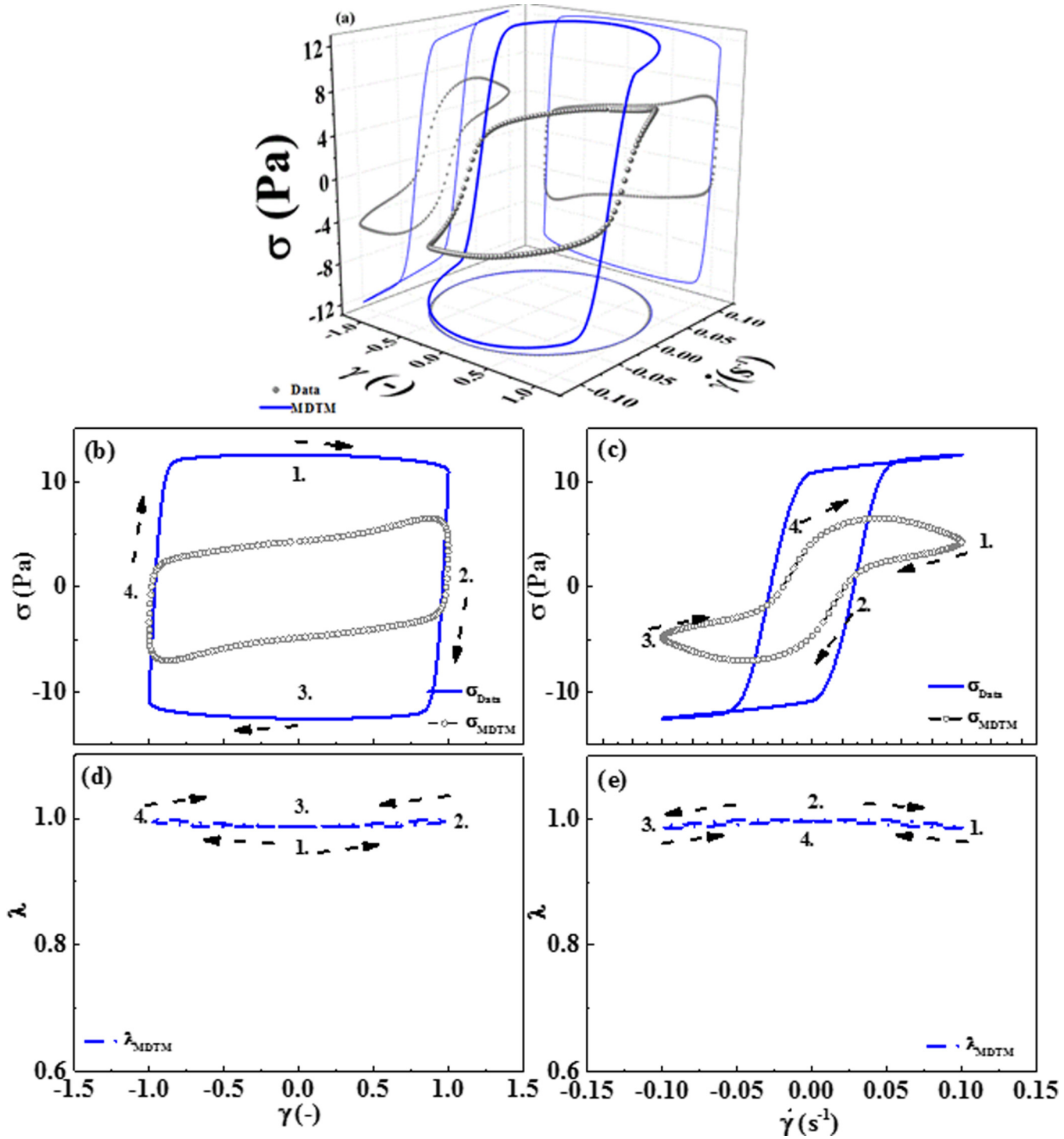

FIG. 10. (a) Three dimensional Lissajous–Bowditch curve $\omega = 0.1\text{rad/s}$; $\gamma_0 = 1$; (b) two dimensional elastic projection; (c) two dimensional viscous projection; (d) two dimensional structural, elastic projection; and (e) two dimensional structural viscous projection. The arrows indicate the direction of time evolution during the cycle and the numbers correspond to specific states discussed in the text.

The conditions shown in Fig. 9 give rise to states where both elastic stresses and viscous stresses are of significance at points during the cycle, and the frequency is such that the suspension's structure can recover significantly during the cycle at alternance. Thus, these conditions provide a good illustration of the rich LAOS behavior of thixotropic suspensions and a good test of model fidelity. At the high shear rates of states 1 and 3, the stress is largely viscous in nature. Reducing the strain rate to zero at the point of flow reversal (states 2 and 4) shows small differences in stress response during the cycle depending on the position due to hysteresis in structure rebuilding and breakdown. Note that the data and the model predictions both cross during the cycle in the viscous projection [see Fig. 9(c)]. The nonzero stress at zero shear rate is characteristic of the yield stress corresponding to structure in the suspension. It is evident that the MDTM can qualitatively capture these effects and supports the typical microstructural interpretation through predictions of the

Redistribution subject to SOR license or copyright; see http://scitation.aip.org/content/sor/journal/jor2/info/about. Downloaded to IP: 128.175.82.78 On: Fri, 01 Apr 2016 15:11:45

structure evolution [Figs. 9(d) and 9(e)]. Importantly, the thixotropic loop evident in the LAOS stress response is also evident in the structure parameter, which lags over the instantaneous shear rate.

Reducing the frequency and strain amplitude each by an order of magnitude locates the LAOS conditions at sufficiently small strain rates and strains such that the experiment is largely dominated by the elasticity leading to the yield stress. Note that this strain value is still above γ_{CO}, such that the suspension is in the weakly nonlinear regime. The experimental data show predominantly elastic behavior with a stress overshoot and viscous flow evident as the maximum shear rates are reached (states 1 and 3). Very significant differences in stress at the states corresponding to flow reversals during the cycle (states 2 and 4) are a consequence of the yield stress. Figures 10(d) and 10(e) show that the sample remains nearly fully structured during the oscillation, such that the model's response is dominated by the yield stress. Note that the model again qualitatively captures the stress overshoot, but now incorrectly predicts a loop in the viscous projection. This can be seen as a large overestimation of the yield stress as evident in the elastic projection [Fig. 10(a)], where the model lies well outside the experimental data. Similar observations were reported in recent experimental studies of colloidal gels by Kim *et al.* [28], where LAOS was shown to result in different structure at alternance as compared to that observed during a comparable steady shear flow.

A global summary of the LAOS experiments and MDTM predictions are presented in the form of Pipkin diagrams in Fig. 11. The gold boxes identify the two frequency and strain amplitude combinations that are shown in Figs. 9 and 10. Not surprisingly, progressing to lower frequencies but higher strain amplitudes (i.e., increasing the maximum shear rate) leads to better model agreement as the stress response is dominated by the viscous behavior of a relatively unstructured material. However, as γ_0 is decreased or ω is increased the structure of the material becomes more and more relevant and the suspension's elastic response dominates the stress signal. For example, at an angular frequency of 1 rad/s and a strain amplitude of 10, the MDTM is able to accurately predict the Lissajous–Bowditch curve, even predicting the secondary loops evident in the viscous projection with the corresponding overshoot evident in the elastic projection. However, when the frequency is reduced to 0.1 rad/s and the strain amplitude is 1, the model is less accurate and misses qualitative features of the data. The maximum stress predicted is about twice the measured stress, and there are no secondary loops evident in the viscous projections of the data while the model predicts minor secondary loops. From Fig. 11 it can be observed that the MDTM consistently overpredicts the maximum stress at low frequency and strain amplitude, which we believe is due to the over-prediction of the structure, coupled with a simple isotropic model for the elastic stresses. Similar results are seen with the SST model, UA

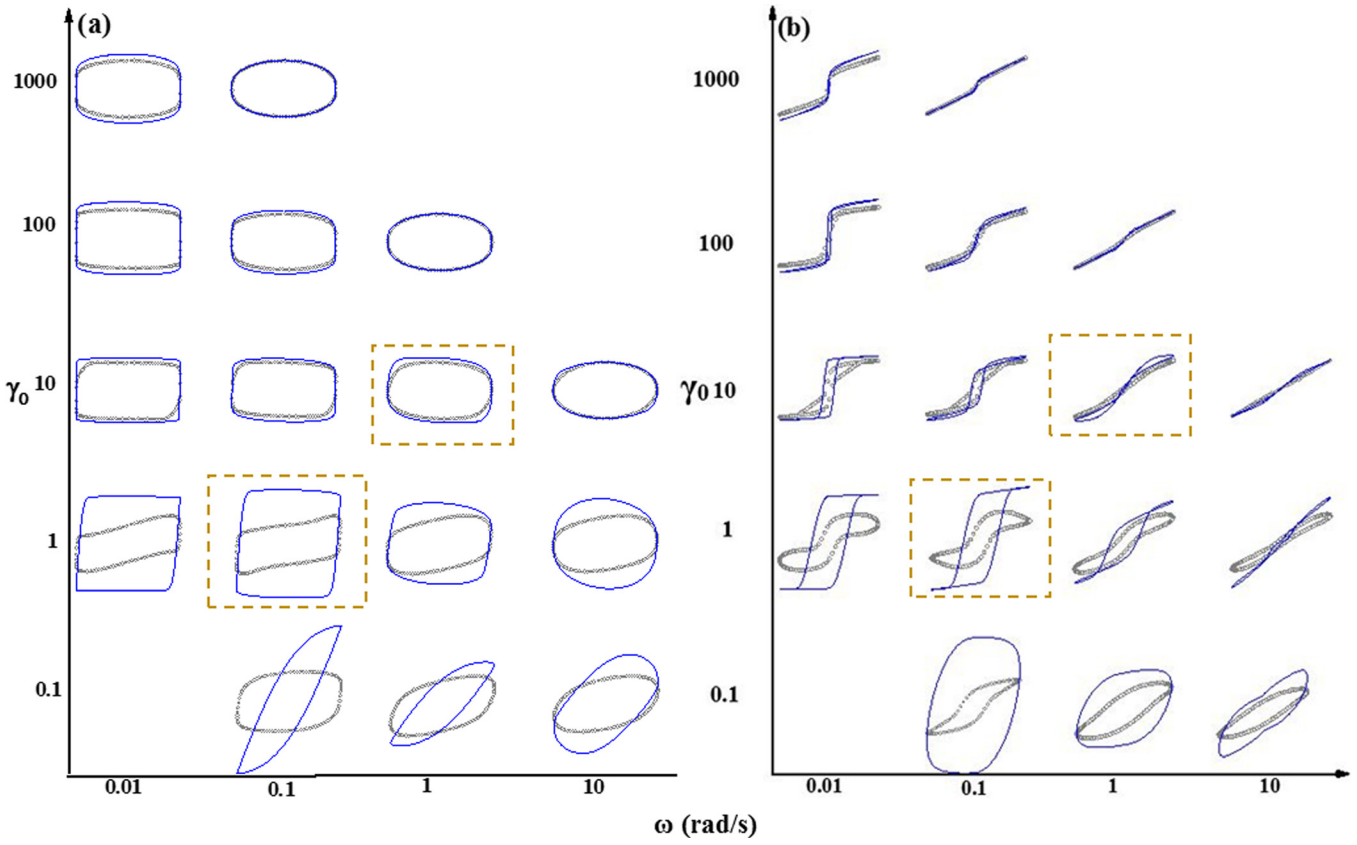

FIG. 11. Pipkin diagram: (a) Elastic projections. (b) Viscous projections. Data (gray open circles) and MDTM predictions (blue lines). The data are made dimensionless by maximum values, while the model predictions are made dimensionless by the same maximum values used for the data. The boxes (gold dashed frames) indicate the states shown in Figs. 9 and 10.

Redistribution subject to SOR license or copyright; see http://scitation.aip.org/content/sor/journal/jor2/info/about. Downloaded to IP: 128.175.82.78 On: Fri, 01 Apr 2016 15:11:45

model, and BMPM LAOS predictions shown in Figs. S.14 and S.15.

This analysis shows that the MDTM can quantitatively predict many features of the LAOS response of nearly ideal thixotropic suspensions, especially for states where the viscous response is dominant. The reduction in accuracy for the combination of low frequencies and small strain amplitudes reveals the inadequacy of the phenomenological model to accurately capture the elastic stress contributions and the coupling to structure. This is evident in the SAOS and therefore, it follows that the predictions will not be as accurate at low strain amplitudes, where the structure is dominant. This leads to the second conclusion, namely that careful consideration is required in order to use LAOS measurements for determining model parameters in constitutive equations.

We compare in Fig. 12 predictions of all four models for the two states considered in Figs. 9 and 10. All four models provide reasonable, quantitative predictions, but differences are apparent. Most strikingly, the UA model predicts significant stress overshoots leading to a "duck head" pattern in the viscous projection that is not evident or so pronounced in the other models or the data. Note that all of the models are capable of parameter tuning to better fit a given LAOS data set, but this will not yield good predictions for other flow conditions. Here, we focus on predictions of LAOS with model parameters independently optimized to fit the steady shear, SAOS, and step-up/down shear data.

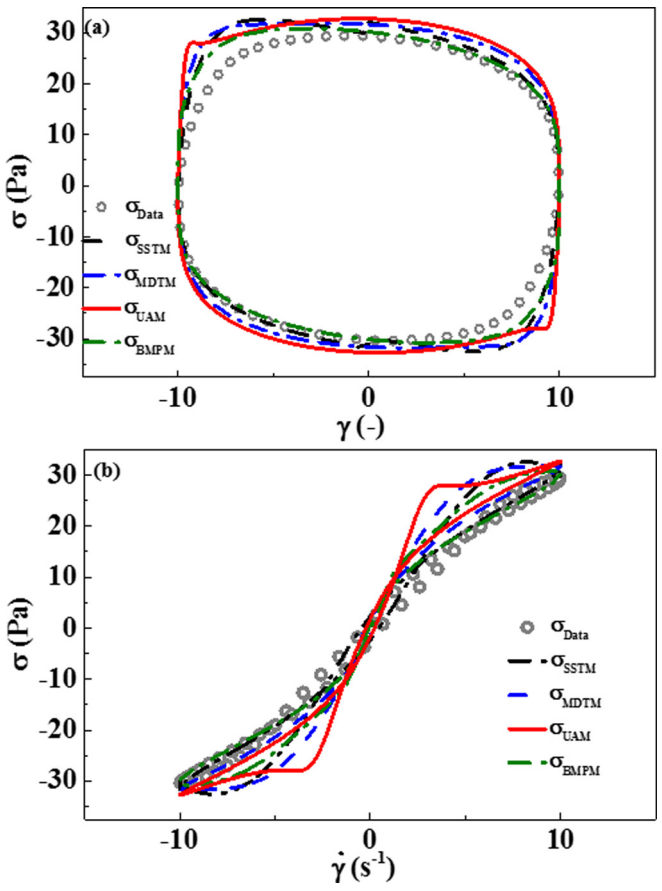

FIG. 12. (a) Elastic projection and (b) viscous projection of all four models at $\omega = 1\text{rad/s}$; $\gamma_0 = 10$.

Similar trends as observed for the MDTM in Fig. 10 were also evident for the other three models explored in this work, with the results for the other models shown in detail in the Supplementary Material [44] (Figs. S.14 and 15). All of the models offer poor predictive capability for conditions of smaller values of strain amplitude and frequency where the yield stress dominates the suspension's response, while all of the models offer more accurate predictions at large strain amplitudes and frequencies, where the material structure is no longer relevant. There is clearly a deficiency in all of the models to predict LAOS behavior at the region where elastic forces are important.

LAOS provides an important distinction in experimental conditions as compared with the steady and transient shear experiments used to derive the model parameters. During LAOS, the direction of the shear rate reverses twice per oscillatory cycle. Such reversals in flow direction are not properly captured by scalar thixotropy models, such as those used in the present work [1,11]. All of the data used for fitting, with the exception of the SAOS, were for unidirectional shear flows and SAOS are asymptotically close to equilibrium. In the following, we explore the hypothesis that the striking differences observed in this work and others [28] comparing the behavior of thixotropic suspensions under LAOS and transient, but unidirectional shear flows, is a consequence of the structural anisotropy induced by shear flow.

B. Flow reversal and unidirectional LAOS experiments

Classic flow reversal experiments were performed to elucidate the importance of directional structure formation under shear. In this experiment, a steady shear rate is applied until the suspension reaches steady state. A rapid reversal in shear flow is performed to a shear rate equal in magnitude, but opposite direction, and the time dependent stress reported. If the structure were independent of the direction of the applied shear, then reversing the flow would leave the structure, and the magnitude of the shear stress unaltered. Figure 13(a) shows the stress response on a logarithmic time scale, where zero on the x-axis represents the time of reversal, where a significant drop in stress is evident. A comparison is shown in Fig. S.16 for the suspending medium, which is Newtonian and shows no effect of the reversal, indicating the accuracy of the method and instrument used. Thus, from direct experimental observation, the direction of flow is an important consideration for the suspension's response.

Also shown in Fig. 13 are *predictions* of the MDTM that indicate an inability to capture the significant transient observed in the data. A very small transition is predicted in the stress [circled region in Fig. 13(a)] due to the elastic strain dependence of the yield stress, but this occurs over a very small strain and is insignificant on the scale of the observed data. The corresponding structure shows no appreciable change due to flow reversal as the structure depends

Redistribution subject to SOR license or copyright; see http://scitation.aip.org/content/sor/journal/jor2/info/about. Downloaded to IP: 128.175.82.78 On: Fri, 01 Apr 2016 15:11:45

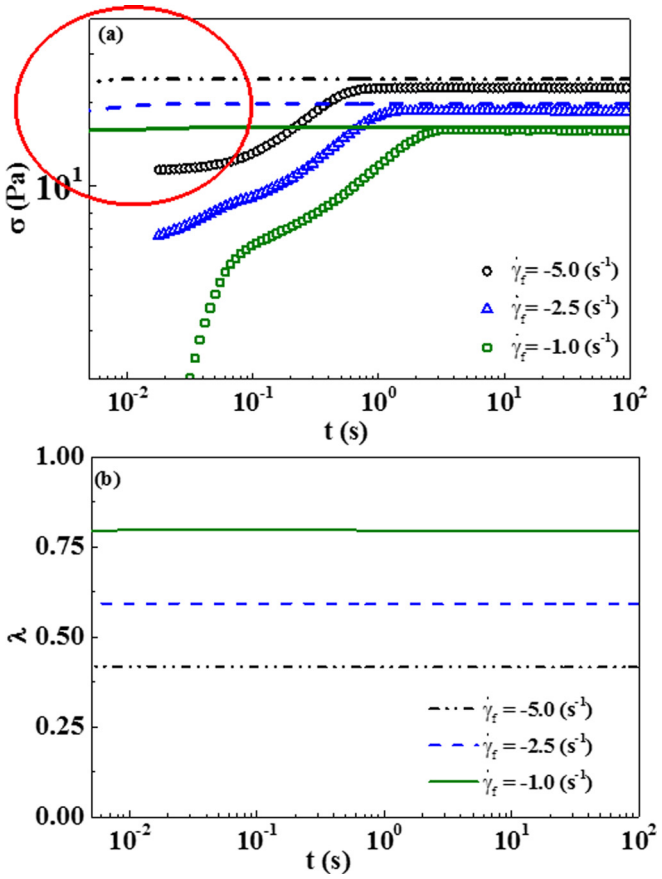

FIG. 13. Flow reversal experiments (a) stress vs time for various shear rates 1, 2.5, and 5 s^{-1} and data (symbols) MDTM (lines) for the rates indicated. The circle highlights the small changes evident in the predictions and (b) MDTM predictions of structure parameter.

only on the magnitude of the shear rate. Analogous flow reversal plots for the other models can be found in the Supplementary Material [44] Fig. S.18, where the SSTM predicts no change while the UAM and BMPM predictions show a transient upon flow reversal. This transient in these models arises from viscoelastic effects. The predictions are qualitatively different than the experimental data in the details of the recovery, which arises primarily from the elastic components of the stress. Thus, all the thixotropy models under investigation here are unable to quantitatively capture the transient stress response in flow reversal. This is conjectured to be caused by the inability of the present models to capture significant structural changes induced by flow reversal.

To further test this hypothesis, we propose and explore here a modified LAOS without flow reversal, termed unidirectional LAOS (UD-LAOS in short). UD-LAOS is more characteristic of pulsatile flows such as physiological blood flow [17]. For UD-LAOS a steady shear flow is superimposed to a LAOS flow at the same shear rate amplitude such that the shear rate oscillates between zero and twice the maximum shear rate of the underlying LAOS flow, thereby never reversing direction. Equations (14) and (15) show the strain and shear rate, respectively,

$$\gamma = \gamma_0 \sin(\omega t) + \gamma_0 \omega t, \tag{14}$$

$$\dot{\gamma} = \gamma_0 \omega \cos(\omega t) + \gamma_0 \omega. \tag{15}$$

Sample UD-LAOS results are shown in Fig. 14 for the same conditions as the LAOS results presented in Figs. 9 and 11, as well as two lower amplitudes where the lowest at $\omega = 1\text{rad/s}; \gamma_0 = 1$, corresponds to LAOS conditions shown in Fig. S.15. To make these comparisons, the experimental data and the model predictions are made comparable to LAOS plots by subtracting out the mean of the experimental stress from each discrete plotted value of stress ($\sigma_{\text{plot}} = \sigma_{\text{exp}} - \bar{\sigma}_{\text{exp}}$), subtracting the continuously evolving average strain ($\omega\gamma_0 t$) from the instantaneous strain, and subtracting the corresponding average background shear rate ($\omega\gamma_0$) from the instantaneous shear rate.

It is apparent that the symmetry of the LAOS curves in these projections is broken by the underlying steady base flow such that states 1–4 [as shown in Figs. 14(a) and 14(b)] are now fundamentally different. The base flow is in the positive direction such that the applied shear rate at state 1 is actually twice that for the corresponding LAOS flow, while that of state 3 is zero. Thus, states 2 and 4 both correspond to states shearing instantaneously with the bulk shear flow, but state 2 is arrived at from a higher shear rate, with less structure, while state 4 is reached from a lower shear rate, with more structure. Correspondingly, the stress in state 2 is lower

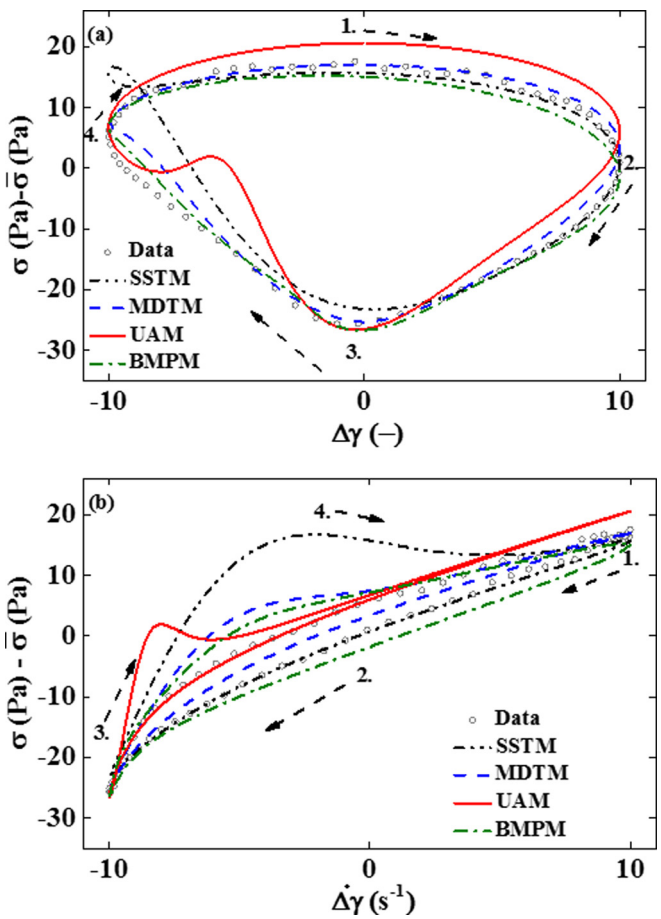

FIG. 14. UD-LAOS data compared to MDTM predictions: (a) Elastic projections and (b) viscous projections $\omega = 1\text{rad/s}; \gamma_0 = 10 (\gamma_0^* = \gamma/\gamma_0;\ \dot{\gamma}_0^* = \dot{\gamma}/\dot{\gamma}_0)$, where $\Delta\sigma = \sigma(t) - \bar{\sigma}(t)$ and $\bar{\sigma}(t) = 26.7\text{Pa}$; $\Delta\gamma = \gamma(t) - \gamma_0\omega t; \Delta\dot{\gamma} = \dot{\gamma}(t) - \gamma_0\omega$.

Redistribution subject to SOR license or copyright; see http://scitation.aip.org/content/sor/journal/jor2/info/about. Downloaded to IP: 128.175.82.78 On: Fri, 01 Apr 2016 15:11:45

than that in state 4 due to a lower degree of structure that has not recovered as much as observed in state 4. Following the cycle from state 1 influenced by the base flow corresponds to transient reduction in the applied shear rate and a corresponding increase in the structure. The applied shear goes to zero at state 4, and the sample is once again undergoing positive shear rate such that the recovering structure is now subject to shear break down as well as shear aggregation. There is a similarity of UD-LAOS to traditional thixotropic loop tests where the shear rate is ramped up and down in the same direction and the stress reported as is used in Bureau *et al*. [16]. An important difference is that UD-LAOS probes a material at alternance rather than a material starting from rest.

Figure 14 compares predictions of all four models using the parameters determined from the steady, SAOS, and unidirectional strain rate jump experiments reported earlier in this manuscript. It can be seen that all four models make significantly more accurate predictions for UD-LAOS than for traditional LAOS flows and that the MDTM gives good predictions. This confirms the importance of directionality of flow in structure determination.

This new set of LAOS, flow reversal and UD-LAOS experiments for a model nearly ideal, thixotropic suspension reveals some important aspects of the coupling of structure to the applied flow; namely, under flow reversal the structure changes significantly and therefore must be anisotropic. This also highlights the possible advantages and disadvantages of using traditional LAOS experiments to probe structured, thixotropic materials, as the flow direction reversals during cycling has a different effect on the structure than setup and step down experiments performed in the same flow direction. We believe that by imposing a LAOS condition the changing flow direction, in addition to the change in shear rate, leads to more nonlinear and complicated effects on the microstructure than our simple models can account for in their present state. This shows that the scalar models in their present form are appropriate to model, and predict only one directional shear flows, but fail to accurately predict the more complicated, LAOS condition or flow reversals.

VI. CONCLUSIONS

This study provides both new experimental data on a nearly ideal, thixotropic system and demonstrates a robust, improved model with significant promise, but limitations on accuracy for weak LAOS flows. New experimental data are presented for a model thixotropic system that significantly extends the data set of Dullaert and Mewis [3]. These new experiments are LAOS, shear flow reversals, and novel UD-LAOS flows, which are shown to be important for rigorously testing models for thixotropic suspensions. The experimental data show only weak viscoelasticity and is reproducible from batch to batch and between laboratories. A very rich LAOS behavior is observed when both viscous stress and yield stress contributions are relevant. This is suggestive of a time-varying structure during alternance, in agreement with recent microstructural observations on a related system [28].

We also present a new thixotropic model based on a scalar structural parameter by modifying the Delaware thixotropic mode [5]. A shear-induced aggregation processes is added in the structure equation and an adaptation of recent improvements in modeling of the yield stress is included in the stress constitutive equation that now explicitly accounts for elastic and plastic deformations. This modified Delaware thixotropy model is found to be superior to three other, representative models from literature as judged by the ability to fit traditional thixotropy measurements consisting of steady-shear flow, SAOS, and rate step-up and step-down flows. All four models are found to have good quantitative predictive capabilities for strong LAOS flows with high shear rate amplitudes, but showed quantitative and qualitative discrepancies for weaker LAOS flows where the contributions from the yield stress dominates. Analysis of these comparisons emphasizes the importance of including three structure kinetic terms corresponding to Brownian and shear aggregation and shear breakup in thixotropic models. The inadequacy of the models to predict LAOS flows where elastic effects predominate was explored. The comparisons also show the difficulties of using LAOS experiments to determine model parameters for thixotropic materials.

The source of the difficulty in predicting LAOS is consistent with similar difficulties in capturing the reversal in flow direction, as demonstrated through exploration of rate reversal experiments. Such deficiencies can be, in part, mitigated by including more elaborate models for the elastic stresses, but ultimately may require a tensorial description of the microstructure. Flow reversal experiments strongly suggest that the structure developing under shear flow is directionally dependent. This is supported by recent experimental observations using flow-SANS in the 1, 2 plane on colloidal gel aggregates showing flow-induced anisotropy [29]. To test this further, we explored a new experiment superimposing a matching steady shear flow with LAOS such that the flow does not reverse during the cycle, termed UD-LAOS. All four thixotropy models are shown to be more successful in predicting UD-LAOS, further confirming the importance of accounting for the direction of flow change in future thixotropy models.

ACKNOWLEDGMENTS

The authors acknowledge the support of the National Science Foundation through Grant No. CBET 312146, the funding assistance from the U.S. Army, and the Department of Chemistry and Life Science, United States Military Academy. Paulo de Souza Mendes (PUC, Brazil) is gratefully acknowledged for significant assistance with the UA models fitting and for helpful suggestions throughout this work. The authors gratefully acknowledge the contributions of Jan Mewis (KU Leuven, emeritus) for help with the model system used in this work, as well as for many helpful suggestions and guidance throughout this work. The views expressed herein are those of the authors and do not reflect the position of the United States Military

Redistribution subject to SOR license or copyright; see http://scitation.aip.org/content/sor/journal/jor2/info/about. Downloaded to IP: 128.175.82.78 On: Fri, 01 Apr 2016 15:11:45

Academy, the Department of the Army, or the Department of Defense.

NOMENCLATURE

a	power law of shear structure breakage term
d	power law of shear aggregation term
$\mathbf{D}$	deformation tensor
F_{OBJ}	objective function
$\mathrm{G_v}(\lambda)$	current value of elastic modulus
G_i	elastic modulus relaxation spectrum values
G_0	elastic modulus
k_G	time scale of elastic modulus evolution
k_i	kinetic constant for structure breaking down of relaxation spectrum i
K_{ST}	consistency (structural)
m	power law of elastic strain
t_{ri}	characteristic thixotropic time scale
γ	applied strain
$\dot{\gamma}$	applied strain rate
γ_{CO}	critical strain
$\eta_{\mathrm{v}}(\lambda)$	current value of viscosity
η_∞	infinite shear viscosity
η_{eq}	equilibrium viscosity
η_{ST}	structural viscosity
θ_1	relaxation time
θ_2	retardation time
λ	structure
λ_i	relaxation time/spectrum values
φ_i	fluidity of relaxation spectrum i
$\varphi_{\infty,i}$	infinite shear fluidity relaxation spectrum i
$\varphi_{0,i}$	zero shear fluidity relaxation spectrum i
σ	shear stress
$\boldsymbol{\sigma}$	stress tensor
σ_e	elastic stress
σ_v	viscous stress
σ_{yd}	dynamic yield stress
σ_{y0}	yield stress

References

[1] Mewis, J., and N. J. Wagner, "Thixotropy," Adv. Colloid Interface Sci. **147–148**, 214–227 (2009).

[2] Larson, R. G., "Constitutive equations for thixotropic fluids," J. Rheol. **59**, 595–611 (2015).

[3] Dullaert, K., and J. Mewis, "A structural kinetics model for thixotropy," J. Non-Newtonian Fluid Mech. **139**(1–2), 21–30 (2006).

[4] Dullaert, K., and J. Mewis, "A model system for thixotropy studies," Rheol. Acta **45**, 23–32 (2005).

[5] Mujumdar, A., A. N. Beris, and A. B. Metzner, "Transient phenomena in thixotropic systems," J. Non-Newtonian Fluid Mech. **102**, 157–178 (2002).

[6] Apostolidis, A. J., M. J. Armstrong, and A. N. Beris, "Modeling of human blood rheology in transient shear flows," J. Rheol. **59**, 275–298 (2015).

[7] de Souza Mendes,P. R., and R. L. Thompson, "A unified approach to model elasto-viscoplastic thixotropic yield-stress materials and apparent yield-stress fluids," Rheol. Acta **52**, 673–694 (2013).

[8] Bautista, F., J. M. de Santos, J. E. Puig, and O. Manero, "Understanding thixotropic and antithixotropic behavior of viscoelastic micellar solutions and liquid crystalline dispersions," J. Non-Newtonian Fluid Mech. **80**, 93–113 (1999).

[9] Mewis, J., and N. J. Wagner, *Colloidal Suspension Rheology* (Cambridge University Press, Cambridge, 2012).

[10] Dullaert, K., "Constitutive equations for thixotropic dispersions," Ph.D. thesis, Katholieke Universiteit Leuven, Leuven, Belgium, 2005.

[11] Mewis, J., "Thixotropy—A general review," J. Non-Newtonian Fluid Mech. **6**, 1–20 (1979).

[12] Morrison, F., *Understanding Rheology* (Oxford University, New York, 2001).

[13] Koopman, D. C., "Review of rheology models for Hanford waste blending," Report No. SRNL-STI-2013-00423, Revision 0. 1-16, Department of Energy, 2013.

[14] Lichtenstein, N. D., "The Hanford nuclear waste site: A legacy of risk, cost, and inefficiency," Nat. Resour. J. **44**, 809–838 (2004).

[15] Bureau, M., J. C. Healy, D. Bourgoin, and M. Joly, "Etude rhéologique en régime transitoire de quelques échantillons de sangs humains artificiellement modifies," Rheol. Acta **18**, 756–768 (1979).

[16] Bureau, M., J. C. Healy, D. Bourgoin, and M. Joly, "Rheological hysteresis of blood at low shear rate," Biorheology **17**, 191–203 (1980).

[17] Sousa, P. C., J. Carneiro, R. Vaz, A. Cerejo, F. T. Pinho, M. A. Alves, and M. S. N. Oliveira, "Shear viscosity and nonlinear behavior of whole blood under large amplitude oscillatory shear," Biorheology **50**, 269–282 (2013).

[18] Grmela, M., A. Ammar, F. Chinesta, and G. Maitrejean, "A mesoscopic rheological model of moderately concentrated colloids," J. Non-Newtonian Fluid Mech. **212**, 1–12 (2014).

[19] Cranford, S.: M. J. Buehler, "Coarse-graining parameterization and multiscale simulation of hierarchical systems," in *Multiscale Modeling: From Atoms to Devices* (CRC, Boca Raton, FL, 2010), Chap. 2.

[20] Goodeve, C. F., "A general theory of thixotropy and viscosity," Trans. Faraday Soc. **35**, 342–358 (1939).

[21] Barnes, H., "Thixotropy—A review," J. Non-Newtonian Fluid Mech. **70**, 1–33 (1997).

[22] Moore, F., "The rheology of ceramic slips and bodies," Trans. Br. Ceram. Soc. **58**, 470–494 (1959).

[23] Fredrickson, A. G., "A model for the thixotropy of suspensions," AIChE J. **16**(3), 436–441 (1970).

[24] de Souza Mendes, P. R., "Modeling the thixtropic behavior of structured fluids," J. Non-Newtonian Fluid Mech. **164**, 66–75 (2009).

[25] Roussel, N., R. Le Roy, and P. Coussot, "Thixotropy modelling at local and macrostcopic scales," J. Non-Newtonian Fluid Mech. **117**, 85–95 (2004).

[26] Coussot, P., A. I. Leonov, and J. M. Piau, "Rheology of concentrated dispersed systems in a low molecular weight matrix," J. Non-Newtonian Fluid Mech. **46**, 179–217 (1993).

[27] Bird, B. R., R. C. Armstrong, and O. Hassager, *Dynamics of Polymeric Liquids* (John Wiley and Sons, New York, NY, 1987).

[28] Kim, J. M., A. P. R. Eberle, A. K. Gurnon, L. Porcar, and N. J. Wagner, "The microstructure and rheology of a model, thixotropic nanoparticle gel under steady shear and large amplitude oscillatory shear (LAOS)," J. Rheol. **58**(5), 1301–1328 (2014).

[29] Eberle, A. P. R., and L. Porcar, "Flow-SANS and Rheo-SANS applied to soft matter," Curr. Opin. Colloid Interface Sci. **17**, 33–43 (2012).

[30] Pignon, F., A. Magnin, and J. Piau, "Butterfly light scattering of a sheared thixotropic clay gel," Phys. Rev. Lett. **79**(23), 4689–4692 (1997).

[31] De Bruyn, J. R., F. Pignon, E. Tsabet, and A. Magnin, "Micron-scale origin of the shear-induced structure in Laponite-poly(ethylene oxide) dispersions," Rheol. Acta **47**, 63–73 (2007).

Redistribution subject to SOR license or copyright; see http://scitation.aip.org/content/sor/journal/jor2/info/about. Downloaded to IP: 128.175.82.78 On: Fri, 01 Apr 2016 15:11:45

[32] Xu, B., and J. F. Gilchrist, "Microstructure of sheared monosized colloidal suspensions resulting from hydrodynamic and electrostatic interactions," J. Chem. Phys. **140**, 204903 (2014).
[33] Lin, N. Y. C., J. H. McCoy, X. Cheng, B. Leahy, J. N. Israelachvili, and I. Cohen, "A multi-axis confocal rheoscope for studying shear flow of structured fluids," Rev. Sci. Instrum. **85**, 033905 (2014).
[34] von Smoluchowski, M., "Experiments on a mathematical theory of kinetic coagulation of colloid solutions," Z. Phys. Chem. Stoechiom. Verwandtschaftsl. **92**(2), 129–168 (1917).
[35] von Smoluchowski, M., "Theoretical observations on the viscosity of colloides," Kolloid-Z. **18**(5), 190–195 (1916).
[36] Dullaert, K., and J. Mewis, "Thixotropy: Build-up and breakdown curves during flow," J. Rheol. **49**(6), 1213–1230 (2005).
[37] Dimitriou, C. J., R. H. Ewoldt, and G. H. McKinley, "Describing and prescribing the constitutive response of yield stress fluids using large amplitude oscillatory shear stress (LAOStress)," J. Rheol. **57**(1), 27–70 (2013).
[38] Giacomin, A. J., and J. M. Dealy, Large-amplitude oscillatory shear, *Techniques in Rheological Measurement* (Chapman and Hall, London, 1993).
[39] Jacob, A. R., A. P. Deshpande, and L. Bouteiller, "Large amplitude oscillatory shear of supramolecular materials," J. Non-Newtonian Fluid Mech. **206**, 40–56 (2014).
[40] Stickel, J. J., J. S. Knutsen, and M. W. Liberatore, "Response of elastoviscoplastic materials to large amplitude oscillatory shear flow in parallel-plate and cylindrical-Couette geometries," J. Rheol. **57**(6), 1569–1596 (2013).
[41] Cheddadi, I., P. Saramito, and F. Graner, "Steady couette flows of elastoviscoplastic fluids are nonunique," J. Rheol. **56**(1), 213–239 (2012).
[42] Saramito, P., "A new elastoviscoplastic model based on the Herschel-Bulkley viscoplastic model," J. Non-Newtonian Fluid Mech. **158**, 154–161 (2009).
[43] Blackwell, B. C., and B. R. Ewoldt, "A simple thixotropic-viscoelastic constitutive model produces unique signatures in large-amplitude oscillatory shear (LAOS)," J. Non-Newtonian Fluid Mech. **208–209**, 27–41 (2014).
[44] See supplementary material at http://dx.doi.org/10.1122/1.4943986 additional rheological experiments showing the determination of the elastic stresses and the linear viscoelastic regime, as well as extensive model comparisons and tables of model parameter values along with comparisons of fits and predictions to steady and transient flows, LAOS, flow reversals, and UD-LAOS experiments. A complete digital compilation of the experimental data presented in this manuscript is also included in the form of an excel workbook.
[45] Philippoff, W., "Vibrational measurements with large amplitudes," Trans. Soc. Rheol. **10**(1), 317–334 (1966).
[46] Gurnon, A. K., C. R. Lopez-Barron, A. P. R. Eberle, L. Porcar, and N. J. Wagner, "Spatiotemporal stress and structure evolution in dynamically sheared polymer-like micellar solutions," Soft Matter **10**, 2889–2898 (2014).
[47] Rogers, S., J. Kohlbrecher, and M. P. Lettinga, "The molecular origin of stres generation in worm-like micelles, using a rheo-SANS approach," Soft Matter **8**, 7831–7839 (2012).
[48] Helgson, M. E., L. Porcar, C. Lopez-Barron, and N. J. Wagner, "Direct observation of flow-concentration coupling in a shear-banding fluid," Phys. Rev. Lett. **105**, 084501 (2010).
[49] Lin, N. Y. C., X. Cheng, and I. Cohen, "Biaxial shear of confined colloidal hard spheres: the structure and rheology of the vorticity-aligned string phase," Soft Matter **10**, 1969–1976 (2014).
[50] Ewoldt, R. H., A. E. Hosoi, and G. H. Mc Kinley, "New measures for characterizing nonlinear viscoelasticity in large amplitude oscillatory shear," J. Rheol. **52**(6), 1427–1458 (2008).
[51] Cho, S. K., K. Hyun, K. H. Ahn, and S. J. Lee, "A geometrical interpretation of large amplitude oscillatory shear response," J. Rheol. **49**(3), 747–758 (2005).
[52] Rogers, S. A., "A sequence of physical processes determined and quantified in LAOS: An instantaneous local 2D/3D approach," J. Rheol. **56**(5), 1129–1151 (2012).
[53] Hyun, K., M. Wilhelm, C. O. Klein, S. C. Kwang, R. H. Ewoldt, and G. H. McKinley, "A review of nonlinear oscillatory shear tests: Analysis and application of large amplitude oscillatory shear (LAOS)," Prog. Polym. Sci. **36**, 1697–1753 (2011).
[54] Gurnon, A. K., and N. J. Wagner, "Large amplitude oscillatory shear (LAOS) measurements to obtain constitutive equation model parameters: Giesekus model of banding and nonbanding wormlike micelles," J. Rheol. **56**(2), 333–351 (2012).
[55] Russel, W. B., N. J. Wagner, and J. Mewis, "Divergence in the low shear viscosity for Brownian hard-sphere dispersions: At random close packing or the glass transition?," J. Rheol. **57**(6), 1555–1567 (2013).
[56] Armstrong, M. J., "Investigating and modeling the thixotropic behavior, microstructure, and rheology of complex material," Ph.D. thesis, University of Delaware, Newark, DE, 2015.
[57] Ogunnaike, B. A., *Random Phenomena Fundamentals of Probatility and Statistics for Engineers* (CRC, Boca Raton, FL, 2010).
[58] Dullaert, K., and J. Mewis, "Stress jumps on weakly flocculated dispersions: Steady state and transient results," J. Colloid Interface Sci. **287**, 542–551 (2005).
[59] O'Brien, V. T., and M. E. Mackay, "Stress components and shear thickening of concentrated hard sphere suspensions," Langmuir **16**(21), 7931–7938 (2000).
[60] Shih, W. H., W. Y. Shih, S. I. Kim, J. Liu, and I. A. Aksay, "Scaling behavior of the elastic properties of colloidal gels," Phys. Rev. A **42**(8), 4772–4779 (1990).
[61] de Souza Mendes, P. R., R. L. Thompson, A. A. Alicke, and R. T. Leite, "The quasilinear large-amplitude viscoelastic regime and its significance in the rheological characterization of soft matter," J. Rheol. **58**, 537–561 (2014).

Redistribution subject to SOR license or copyright; see http://scitation.aip.org/content/sor/journal/jor2/info/about. Downloaded to IP: 128.175.82.78 On: Fri, 01 Apr 2016 15:11:45